RHYTHMOMIMETIC DRUG DELIVERY: MODELING, ANALYSIS AND NUMERICAL SIMULATION

LINGXING YAO

DEPARTMENT OF MATHEMATICS, APPLIED MATHEMATICS AND STATISTICS

CASE WESTERN RESERVE UNIVERSITY

CLEVELAND, OH 44106

AND

M. CARME CALDERER AND YOICHIRO MORI

SCHOOL OF MATHEMATICS

AND

RONALD A. SIEGEL

DEPARTMENTS OF PHARMACEUTICS AND BIOMEDICAL ENGINEERING

UNIVERSITY OF MINNESOTA, MINNEAPOLIS, MN 55455

Abstract. We develop, analyse and numerically simulate a model of a prototype, glucose-driven, rhythmic drug delivery device, aimed at hormone therapies, and based on chemomechanical interaction in a polyelectrolyte gel membrane. The pH-driven interactions trigger volume phase transitions between the swollen and collapsed states of the gel. For a robust set of material parameters, we find a class of solutions of the governing system that oscillate between such states, and cause the membrane to rhythmically swell, allowing for transport of the drug, fuel and reaction products across it, and collapse, hampering all transport across it. The frequency of the oscillations can be adjusted so that it matches the natural frequency of the hormone to be released. The work is linked to extensive laboratory experimental studies of the device built by Siegel's team. The thinness of the membrane and its clamped boundary, together with the homogeneously held conditions in the experimental apparatus, justify neglecting spatial dependence on the fields of the problem. Upon identifying the forces and energy relevant to the system, and taking into account its dissipative properties, we apply Rayleigh's variational principle to obtain the governing equations. The material assumptions guarantee the monotonicity of the system and lead to the existence of a three dimensional limit cycle. By scaling and asymptotic analysis, this limit cycle is found to be related to a two-dimensional one that encodes the volume phase transitions of the model. The identification of the relevant parameter set of the model is aided by a Hopf bifurcation study of steady state solutions.

1. Introduction. Research on drug delivery systems is focused on presenting drug at the right place in the body at the right time [33]. To this end, we have introduced a prototype chemomechanical oscillator that releases GnRH in rhythmic pulses, fueled by exposure to a constant level of glucose [2, 9, 15]. Experience with chemical and biochemical oscillators [16], [11] and [14], and with electrical and mechanical relaxation oscillators [1], shows that rhythmic behavior can be driven by a constant rate stimulus, provided proper delay, memory and feedback elements are employed in device dynamics. The device consists of two fluid compartments, an external cell (I) mimicking the physiological environment, and a closed chamber (II), separated from (I) by a hydrogel membrane. Cell I, which is held at constant pH and ionic strength, provides a constant supply of glucose to cell II, and also serves as clearance station for reaction products. Cell II contains the drug to be delivered to the body, an enzyme that catalyzes conversion of glucose into hydrogen ions, and a piece of marble to remove excess hydrogen ions that would otherwise overwhelm the system. When the membrane is swollen, glucose flux into Cell II is high, leading to rapid production of hydrogen ions. However, these ions are not immediately released to Cell I but react, instead, with the negatively charged carboxyl groups of the membrane, which collapses when a critical pH is reached in Cell II, substantially attenuating glucose transport and production of ions. Subsequent diffusion of membrane attached H-ions increases again the concentration of negative carboxyl groups in the membrane, causing the gel to reswell, and so, the process is poised to repeat itself. Since drug release can only occur when the membrane is swollen, it occurs in rhythmic pulses that are coherent with the pH oscillations in Cell II and swelling oscillations of the membrane.

While rhythmic hormone release across the membrane is the ultimate goal of this research, a main purpose of this article is the study of the pH oscillations in Cell II. These oscillations correlate with those of H^+ concentration in the membrane, which determine its swelling state.

A polyelectrolyte gel is a mixture of polymer and fluid, the latter containing several species of ions and the polymer including electrically charged (negative) side groups. We model the gel as an incompressible, saturated mixture of polymer and fluid. The hydrogel (polyelctrolyte gel having water as the fluid solvent) of the experimental device is a relatively thin membrane that is laterally restrained by clamping justifying its treatment as a one-dimensional system. Moreover, the experimental apparatus is kept well-stirred at all times, allowing for further reduction to a time-dependent, spatially homogeneous system. The system consists of three coupled mechanical-chemical ordinary differential equations for the time evolution of the membrane thickness $L = L(t)$, the hydrogen concentrations $x(C_H^M)$ and $z(C_H^{II})$ inside the membrane and in the chamber, respectively. The polymer volume fraction $\phi(t)$ is related to $L(t)$ by the equation of balance of mass of the polymer, $L = \frac{\phi_0}{\phi}$, where ϕ_0 denotes the corresponding volume fraction in the reference state of the membrane. The governing system also takes into account the algebraic constraint of electroneutrality. Analysis and simulation of gel swelling in higher dimensional geometries, in the purely mechanical case, have been carried out in [6] and [26].

The swelling force in the hydrogel consists of mixing, elastic and ionic terms [10, 13]. The first two terms are derived from the Flory-Huggins energy of mixing and the neo-Hookean form of the elastic stored energy, respectively. The combination of Lagrangian elasticity and Eulerian mixing energies gives rise to the well known Flory-Rehner theory. The ionic force follows Van't Hoff's ideal law. The latter force depends on the degree of ionization due to acid-base equilibria between pendant ionizable groups in the hydrogel and free hydrogen ion, as described by a Langmuir isotherm, and the resulting Donnan partitioning of counterions and co-ions into the hydrogel. Taking all these factors into account, we call the model for swelling stress the Flory-Rehner-Donnan-Langmuir (FRDL) model.

A scaling analysis reveals that, of the many physical parameters of the model, five dimensionless parameter, $\mathcal{A}_i$, encode most mechanical and chemical properties of the system. These together with control parameters such as salt concentration C_{NaCl}, reaction rate constant of the marble k_{mar}, degree of ionization of the polymeric side groups σ_0, reference polymer volume fraction ϕ_0 and degree of polymer cross-linking ρ_0 are sufficient to fully describe the evolution properties of the system.

A study of the stationary states of the system shows the hysteretic behavior for appropriate parameter ranges that is consistent with laboratory experiments [21, 4, 3]. Moreover, we find that, for every set of parameters within the relevant range, there exists a unique steady state that is hyperbolic. We study the Hopf bifurcation of the steady state and numerically identify the parameter regions within which oscillations occur. We found these regions to be in good agreement with experiment.

Dimensionless parameter groups determine the relative time scales of the system, with the fast time corresponding to the swelling ratio of the membrane. In particular, this implies that solutions of the governing system remain arbitrarily close to those of a suitable two dimensional system, for most of the time. Although the original system has positive C^1-solutions with ϕ bounded away from 0 (and ϕ bounded away from 1, as well), the two-dimensional restriction involves multivalued functions, leading to existence of weak solutions, with discontinuous ϕ and, consequently, the swelling ratio being discontinuous as well. The latter corresponds to a volume phase transition taking place that drives the permeability changes of the membrane. The Poincaré-Bendixon theory for plane systems applies to the current problem from which existence of a two-dimensional limit cycle follows. It turns out that the limit cycle is also the omega-limit set of positive semi-orbits of the full system.

In order to show existence of a limit-cycle of the three dimensional system, we must appeal to the theory of monotone dynamical systems. Specifically, we show that our three dimensional system is competitive with respect to a properly defined alternate cone, that results from the intersection of half-spaces. We also find that the Jacobian matrix of the system satisfies the properties of *sign-stability* and *sign-symmetry*, from which existence of a three-dimensional limit cycle follows. It turns out that our system is qualitatively analogous to that modeling the dynamics of the HIV in the regime where the concentrations of infected and uninfected T-cells and the virus follow a periodic holding pattern, away from the fully infected state represented by a hyperbolic steady state [25].

The outline of this paper is as follows. In section 2, we describe the prototype oscillator and outline its basis for operation. In section 3, we study the mechanical and chemical properties of the system. The assumptions of the model and the subsequent formulation of a precursory system of ordinary differential equations are presented in section 4. In section 5, we describe the parameters of the system and explore its scaling properties, from which the system of ordinary differential equations that model the dynamics of
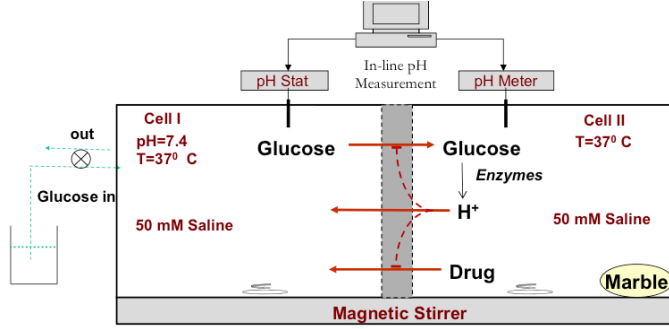
Fig. 2.1. *Diagram of the Experimental Oscillator [2, 15]*

the oscillator follows. The Hopf bifurcation analysis of the unique hyperbolic equilibrium point is presented in section 6. In section 7, we construct an inertial manifold of the three-dimensional system and analyze the corresponding two-dimensional flow in the manifold, demonstrating existence of an asymptotically stable limit cycle. In section 8, we study the monotonicity properties of the system and prove the existence of a three-dimensional limit cycle. A multiscale, asymptotic analysis is developed in section 9 that yields decay estimates of solutions as they approach the two-dimensional manifold, where hysteresis properties manifest themselves, including the canàrd feature of the system. We conclude with a discussion of the benefits and deficiencies of the present model.

2. Rhythmic Hormone Delivery: A Simple Experimental System. A simplified schematic representation of the experimental oscillator is depicted in Figure 1 [2, 15]. The apparatus consists of two well stirred fluid compartments, or cells, separated by a sweallable hydrogel membrane. Cell I, which is meant to mimic the external physiological fluid environment, contains glucose in saline solution, with fixed glucose concentration maintained by introduction of fresh medium and removal of reaction products by flow, and fixed pH 7.0 enforced by a pH-stat servo (autotitrating burette). Cell II, which simulates the interior of the rhythmic delivery device, contains the hormone to be released (e.g. GnRH) and the enzymes glucose oxidase, catalase, and gluconolactonase, which catalyze conversion of glucose to gluconic acid. The latter rapidly dissociates into hydrogen ion (H^+) and gluconate ion:

$$\text{Glucose} + O_2 \xrightarrow{enzymes} H^+ + \text{Gluconate}^- + \frac{1}{2}O_2 \text{ (I)}$$
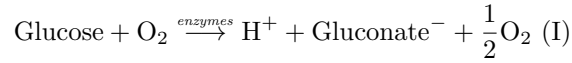
Cell II also contains physiologic saline, which is exchanged with Cell I through the membrane, and a piece of solid marble. Marble is solid calcium carbonate, $CaCO_3(s)$, which reacts with H^+ according to

$$2H^+ + CaCO_3(s) \longrightarrow Ca^{2+} + CO_2 \uparrow + H_2O \text{ (II)}$$
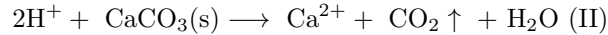
The hydrogel membrane is clamped between Cells I and II. The degree of swelling of the membrane and permeabilities to glucose and GnRH, depend on the internal concentration of H^+ ions, through the reaction [10, 17, 22].

$$\vdash COO^- + H^+ \rightleftharpoons \vdash COOH \text{ (III)}$$
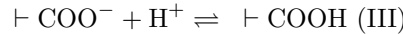
At low H^+ concentration, the membrane is charged, swollen, and highly permeable to both glucose and GnRH, but permeability to these compounds is substantially attenuated at higher H^+ concentrations where the membrane has less charge and is relatively collapsed. The placement of the membrane between a source of fuel, glucose, and its converting enzymes creates a dynamic environment with competing effects. On the one hand, the enzyme reaction produces H^+, which affects the permeability of the membrane; it is removed from the system by reacting with marble, and also by diffusing out to the environment. This creates a negative feedback mechanism between the enzyme reaction and the membrane permeability to glucose. Under proper conditions, this arrangement can lead to oscillations.

When the membrane is ionized and swollen, glucose permeates from Cell I to Cell II and is converted to H^+, which diffuses back into the membrane, binds and neutralizes the $\vdash COO^-$ groups, and causes the

hydrogel membrane to collapse. The membrane is now impermeable to glucose, and enzymatic production of H^+ is attenuated. Eventually the H^+ ions bound to the membrane diffuse into Cell I, where they are neutralized by the pH-stat and removed in the waste stream. The membrane then reionizes and reswells, and the system is primed to repeat the previous sequence of events.

In order to achieve sustained oscillations, a steady state in which flux of glucose, enzyme reaction rate, and flux of H^+ are balanced and equal at all times, must be avoided. As it will be seen, bistability, or hysteresis of membrane swelling response to H^+, provides a means for destabilizing such a steady state.

The reader is referred to experimental details and results in previous publications [2, 9, 15].

3. A Lumped Parameter Model. A full mathematical description of the experimental system just described would require a detailed account of 1) diffusional and convective fluxes of solvent and solutes, 2) the spatial three-dimensional mechanics of the hydrogel membrane which, though constrained by clamps, exhibits swelling and shrinking which is both time and position dependent, 3) the kinetics of enzymatic conversion of glucose to H^+, and 4) the kinetics of binding and dissociation of H^+ with $\vdash COO^-$ groups. An accurate, verifiable model of this sort, which would require partial differential equations to describe intramembrane processes, does not yet exist. Here we simplify the problem by assuming that the membrane is a lumped, uniform element. All mechanical and chemical variables are homogenized to single values representing the whole membrane. We recognize that some potentially important consistencies are lost in this approximation. First, there will always be a difference in pH between Cells I and II, which will lead to intramembrane gradients in the chemical and mechanical variables. Second, self consistent boundary conditions, which would follow naturally from a PDE model, must be replaced by somewhat *ad hoc* assumptions.

As a second simplification, we assume that the enzyme reactions, and the process of distribution of the dominant background electrolyte, NaCl, between Cells I and II and the hydrogel membrane, are very fast compared to the other dynamical processes. These assumptions can be justified, respectively, by the excess of enzyme used in the experiments, and the fact that the capacity of the membrane for acidic protons (H^+, or $\vdash COOH$) relative to Cells I and II, far exceeds its relative capacities for Na^+ and Cl^-. Many experimental studies with polyacidic hydrogels have confirmed that H^+ dynamics and poroelastic relaxations are much slower than those of NaCl [4, 21, 3].

3.1. Swelling of Hydrogels. The membranes considered in this work are crosslinked networks of polymer chains, or hydrogels, which absorb substantial amounts of water. Depending on water content, or degree of swelling, the hydrogel will be more or less permeable to solutes such as glucose and H^+. Hydrogels have a long history of application in drug delivery and medicine due to their mechanical and chemical compatibility with biological tissues and their ability to store and release drugs in response to environmental cues [31].

In the present system, we utilize the hydrogen ions H^+ that are enzymatically generated from glucose to control hydrogel swelling and hence release of hormone. In polyacid hydrogels, swelling is controlled by degree of ionization, which results from dissociation of acidic side groups that are attached to the polymer chains. When NaCl is present in the aqueous fraction of the hydrogel, the ionization equilibrium is represented by

$$\vdash COOH + \ Na^+ + Cl^- \rightleftharpoons \vdash COO^- \ Na^+ + H^+ + Cl^-$$
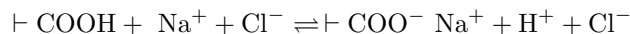
Swelling of a polyacidic hydrogel results from three thermodynamic driving forces [10, 13, 23, 32]. First there is the tendency of solvent (water) to enter the hydrogel and mix with polymer in order to increase translational entropy. The mixing force also depends on the relative molecular affinity or aversion of the polymer for water compared to itself due to short range van der Waals, hydrogen bonding, and hydrophobic interactions. Second, there is an elastic force, which is a response to the change in conformational entropy of the polymer chains that occurs during swelling or shrinking. The third force is due to ionization of the acidic pendant groups, which leads to an excess of mobile counterions and salt inside the hydrogel compared to the external medium, promoting osmotic water flow into the hydrogel. The ion osmotic force acts over a much longer range than the direct polymer/water interaction.

In the present work, it is assumed that the hydrogel is uniform in composition when it is prepared. The hydrogel at preparation is taken as the reference state for subsequent thermodynamic model calculations. At preparation, the volume fraction of polymer in the hydrogel is denoted by ϕ_0. Crosslinking leads to an initial density of elastically active chains, ρ_0. The initial density of ionizable acid groups, fixed to the polymer chains, is denoted by σ_0. Both densities have units mol/L, and are referred to the total volume of the hydrogel (polymer+water) at preparation.

3.2. Mechanics of Swelling. The swelling state of a hydrogel is characterized by the principal stretches or elongation ratios $(\alpha_x, \alpha_y, \alpha_z)$, and the volume fraction ϕ of the polymer. We let $0 < \phi_0 < 1$ and $L_0 > 0$ denote the volume fraction of polymer and the thickness of the membrane, respectively, in the reference state. The equation of conservation of mass of polymer in the gel is

$$\phi = \phi_0(\alpha_x \alpha_y \alpha_z)^{-1}. \tag{3.1}$$

The swelling ratio of the membrane relative to its undeformed reference state is $\phi_0/\phi = \alpha_x \alpha_y \alpha_z$, that is, the Jacobian of the deformation map from the reference to the deformed membrane. We assume that the elongation ratios and volume fraction vary with time. Since in the present system the hydrogel is a relatively thin membrane that is laterally restrained by clamping, we assume that the main swelling effect occurs along the thickness direction. Hence, we consider uniaxial deformations

$$\alpha := \alpha_x, \alpha_y = \alpha_z = 1. \tag{3.2}$$

REMARK 1. *A rigorous justification of the uniaxiality assumption on the membrane deformation may follow from a dimensional reduction analysis. However, a main drawback of the one-dimensional treatment is that it neglects undulating surface instabilities observed in gel free surfaces, which may ultimately hamper sustained oscillatory behaviour.* Denoting by $L = L(t)$ the thickness of the membrane at time $t \geq 0$, equation (3.1) reduces to

$$L\phi = L_0\phi_0. \tag{3.3}$$

In the model presented below, the three swelling forces, mixing, elastic and ionic, yield the uniaxial *swelling stress*,

$$s = s_{\text{mix}} + s_{\text{elast}} + s_{\text{ion}}. \tag{3.4}$$

which reflects the excess free energy density of the hydrogel relative to equilibrium, at a given state of swelling in a prescribed aqueous medium. At equilibrium, $s = 0$. Let g_{mix} and g_{elast} denote the Flory-Huggins mixing and elastic energy densities with respect to deformed volume, respectively. The corresponding total energy quantities, per unit cross-sectional area, are

$$G_{\text{mix}} = Lg_{\text{mix}}(\phi), \quad G_{\text{elast}} = Lg_{\text{elast}}(\phi), \tag{3.5}$$

A standard variational argument gives the dimensionless stress components as

$$s_{\text{mix}} = -\frac{dG_{\text{mix}}}{dL}, \quad s_{\text{elast}} = -\frac{dG_{\text{elast}}}{dL}. \tag{3.6}$$

Consequently,

$$s_i = -(g_i - \phi\frac{\partial g_i}{\partial \phi}), \ i = \text{mix, elast.} \tag{3.7}$$

The mixing free energy density of solvent (water) with the hydrogel chains is modeled according to the Flory-Huggins expression

$$g_{\text{mix}} = \frac{RT}{v_{\text{w}}}[(1-\phi)\ln(1-\phi) + \chi\phi(1-\phi)], \tag{3.8}$$

where R is the gas constant, T is absolute (Kelvin) temperature, and v_{w} is the molar volume of water. The first term in the square brackets accounts for the translational entropy change of solvent molecules as they move from the external environment into the hydrogel, temporarily assuming that the bath is pure solvent. The second term accounts for short range contact interactions between polymer and solvent, summarized by the dimensionless parameter χ, which is the molar free energy required to form solvent/polymer contacts, normalized by RT. Introducing (3.8) into (3.7) yields

$$s_{\text{mix}} = -\frac{RT}{v_{\text{w}}}[\ln(1-\phi) + \phi + \chi\phi^2]. \tag{3.9}$$

In the simplest form of Flory-Huggins theory χ is constant, but in many hydrogel systems, especially those that undergo sharp swelling/shrinking transitions, a pseudo-virial series in ϕ is used. In the present work the series is truncated at the linear term, taking the form [12], [18],

$$\chi = \chi_1 + \chi_2 \phi. \tag{3.10}$$

With $\chi_2 > 0$, polymer and solvent become increasingly incompatible as polymer concentration increases, with hydrogel shrinking, and mixing pressure decreasing.

We model the elastic energy density according to the Neo-Hookean expression

$$g_{\text{elast}} = \frac{RT}{2}\rho_0(\frac{\phi}{\phi_0})(\alpha_x^2 + \alpha_y^2 + \alpha_z^2 - 3 - \ln\alpha_x\alpha_y\alpha_z). \tag{3.11}$$

The logarithmic term accounts for change in entropy of localization of crosslinks in the hydrogel due to swelling. For the uniaxial swelling under consideration,

$$g_{\text{elast}}^{\text{uni}} = RT\rho_0(\frac{\phi}{\phi_0})[(\frac{\phi_0}{\phi})^2 - \ln\frac{\phi_0}{\phi} - 1] \tag{3.12}$$

which upon introduction into (3.7) yields

$$s_{\text{ elast}} = -RT\rho_0(\frac{\phi_0}{\phi} - \frac{\phi}{2\phi_0}). \tag{3.13}$$

Summing (3.9) and (3.13) we obtain the Flory-Rehner expression for the nonionic component of the swelling stress (see also (3.17), below. We now derive the evolution equation of the membrane according to the minimum rate of dissipation principle.

PROPOSITION 3.1. *Suppose that $\phi = \phi(t)$ and $L = L(t)$, $t \geq 0$ satisfy equation (3.3). Let us define the rate of dissipation function and the total energy as*

$$W = \frac{K}{2}(\frac{dL}{dt})^2 \text{ and } E = G_{mix} + G_{elast}, \tag{3.14}$$

respectively, with $K > 0$ denoting a friction coefficient. Then the function $v = \frac{dL}{dt}$ that minimizes the Rayleighian functional $R = \dot{E} + W$, among spatially homogeneous fields, satisfies the equation

$$s_{\text{ mix}} + s_{\text{ elast}} - K\frac{dL}{dt} = 0, \tag{3.15}$$

with $s_{\text{ mix}}$ and $s_{\text{ elast}}$ as in (3.9) and (3.13), respectively, and G_{elast} and G_{mix} as in (3.5). The proof results from the simple calculation

$$\frac{dE}{dt} = \frac{d}{dt}\big(g_{\text{ mix}} + g_{\text{elast}}\big), \quad = -(s_{\text{ mix}} + s_{\text{ elast}})v, \quad v = \frac{dL}{dt}. \tag{3.16}$$

So, the critical points $v = v(t)$ of R satisfy equation (3.15), for all $t \geq 0$. Defining the *permeability coefficient* as $K_{\text{w}} = \frac{RT}{K\nu_w}$, and using equations (3.9) and (3.13), equation (3.15) becomes

$$\frac{dL}{dt} = -K_w[\ln(1-\phi) + \phi + \chi\phi^2 + \nu_w\rho_0(\frac{\phi_0}{\phi} - \frac{\phi}{2\phi_0})]. \tag{3.17}$$

Equation (3.15) should be expanded to include the force $s_{\text{ ion}}$ as in (3.4). The calculation of such a contribution is given next.

3.3. Chemical reactions. While the mixing and elastic terms represent important contributions to swelling pressure, the ionic term responds to H^+ concentration inside the membrane, and this is what forms the basis for the oscillator's dynamic behavior. As described above, ionization of the hydrogel occurs by dissociation of pendant carboxylic acid groups. The fraction of these groups that are ionized, f, is modeled according to a Langmuir isotherm relation,

$$f = \frac{K_{\text{A}}}{K_{\text{A}} + C_{\text{H}}}. \tag{3.18}$$

where C_{H} is the concentration of H$^+$ in the aqueous portion of the hydrogel and K_A is the dissociation constant of the carboxylic acid. The concentration of ionized groups, referenced to the aqueous portion of the hydrogel, is then given by

$$C_{\text{A-}} = f\sigma_0(\phi/\phi_0), \tag{3.19}$$

where σ_0 denotes the reference density of ionized groups fixed to the polymer chains. Letting C_{AH} denote the concentration of H^+ linked to carboxyl groups, the conservation of intra-membrane hydrogen ions is given by the equation

$$L(C_{\text{H}} + C_{\text{AH}}) = L_0\sigma_0. \tag{3.20}$$

Combining equations (3.19) and (3.20) yields

$$C_{\text{AH}} = \frac{\phi}{\phi_0}(1-f)\sigma_0. \tag{3.21}$$

Ionization of hydrogel side-chains, plus the requirement for quasi-electroneutrality over any distance exceeding a few Debye lengths (~ 5 nm in physiological systems) leads to a distribution of mobile ions in the hydrogel that differs from that in the external bath. Ignoring very small contributions from H$^+$ and OH$^-$ ions, a quasineutrality condition is

$$C_{\text{Na}} - C_{\text{Cl}} - C_{\text{A-}} = 0. \tag{3.22}$$

where C_{Na} and C_{Cl} are the concentrations, respectively, of Na$^+$ and Cl$^-$ in the aqueous portion of the hydrogel.

For simplicity, we assume that Cells I and II contain fully dissociated NaCl, with ion concentrations $C'_{\text{Na}} = C'_{\text{Cl}} = C'_{\text{NaCl}}$. Ionic swelling stress in the membrane is modeled using van't Hoff's ideal law:

$$s_{\text{ion}} = RT(C_{\text{Na}} + C_{\text{Cl}} - 2C'_{\text{NaCl}}). \tag{3.23}$$

Derivation of this term from a free energy density expression is possible but not carried out here since the basis for van't Hoff's law is well understood.

It can be shown that diffusion of salt inside the hydrogel is very fast compared to diffusion of H$^+$ and mechanical relaxation of swelling pressure. We may therefore assume that at any point in the hydrogel a Donnan quasi-equilibrium, where $C_{\text{Na}} = \lambda C'_{\text{Na}}$ and $C_{\text{Cl}} = \lambda^{-1}C'_{\text{Cl}}$, with λ the Donnan ratio, determined by combining (3.18)-(3.22), giving

$$(1-\phi)(\lambda - \frac{1}{\lambda})C'_{\text{NaCl}} - \sigma_0(\phi/\phi_0)f = 0. \tag{3.24}$$

With λ in hand, (3.23) becomes

$$s_{\text{ion}} = RT(\lambda + \frac{1}{\lambda} - 2)C'_{\text{NaCl}}. \tag{3.25}$$

Introducing (3.9, 3.10, 3.13, 3.25) into (3.4) gives

$$\frac{v_{\text{w}}s}{RT} = -[\ln(1-\phi) + \phi + (\chi_1 + \chi_2\phi)\phi^2] - v_{\text{w}}\rho_0(\frac{\phi_0}{\phi} - \frac{\phi}{2\phi_0}) + (\lambda + \frac{1}{\lambda} - 2)v_{\text{w}}C'_{\text{NaCl}}, \tag{3.26}$$

which, combined with (3.24), determines the total swelling stress. Rewriting equation (3.17) taking the total stress into account leads to the force balance equation stated in (4.1).

Because (3.26) and (3.24) include elements of Flory-Rehner theory, and Donnan and Langmuir quasi-equilibria, we call these two equations the FRDL model for uniaxial swelling stress. The behavior of this model depends on the hydrogel parameters ϕ_0, ρ_0, σ_0, χ_1, χ_2 and pK_{A}, and the external salt concentration C'_{NaCl}, which is assumed to be constant. These, together with relevant dimensionless parameter groups, determine the swelling and permeability properties of the hydrogel membrane.
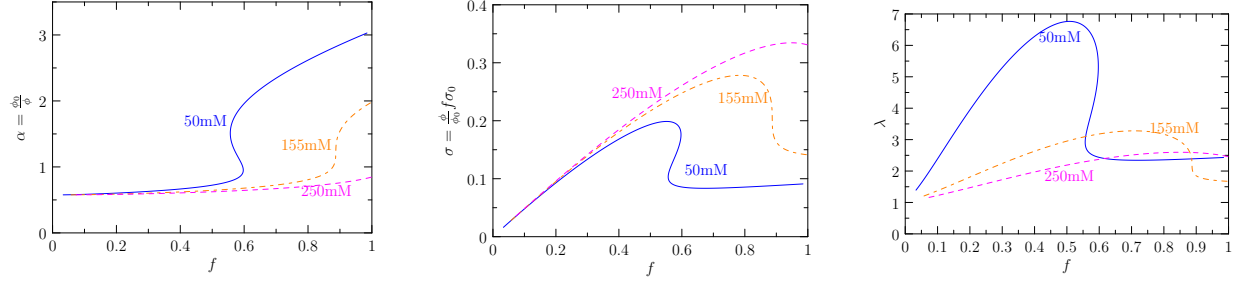
FIG. 3.1. *The left, middle and right figures show the uniaxial swelling ratio α, the fixed charge density σ and the Donnan ratio λ respectively, versus ionized fraction f, for different salt concentration.*

3.4. Swelling equilibria. Before pursuing dynamics, it is useful to examine homogeneous uniaxial swelling equilibria for a hydrogel in a bath of fixed $pH = -\log C'_{\mathrm{H}}$. In this case $s = 0$ in (3.26) and $C_{\mathrm{H}} = \lambda C'_{\mathrm{H}} = \lambda 10^{-pH}$. Setting $pK_{\mathrm{A}} := -\log K_{\mathrm{A}}$, equation (3.24) becomes

$$10^{-(pH-pK_{\mathrm{A}})}(1-\phi)C'_{\mathrm{NaCl}}\lambda^3 + (1-\phi)C'_{\mathrm{NaCl}}\lambda^2 - [10^{-(pH-pK_{\mathrm{A}})}(1-\phi)C'_{\mathrm{NaCl}}$$
$$+\sigma_0(\frac{\phi}{\phi_0})]\lambda - (1-\phi)C'_{\mathrm{NaCl}} = 0. \tag{3.27}$$

We discuss the solvability of equation (3.27) with respect to λ. Since the physical parameters contributing to the polynomial coefficients are positive and $\phi \leq 1$, there is only one sign change in the descending polynomial coefficients, and Descartes' rule of signs mandates a single positive real root. (Negative or complex values of λ are physically meaningless as they would predict negative or complex ion concentrations inside the hydrogel.) Moreover, substituting $\lambda = \nu + 1$ in (3.27) and rearranging terms, we obtain a cubic polynomial in ν that also has only one sign change, hence $\nu \geq 0$ and $\lambda \geq 1$. This makes physical sense, since for negatively charged hydrogel the internal cation concentration must exceed its external counterpart.

The first and third terms of (3.27) can vary over several orders of magnitude with pH, indicating that pH, which affects ionization, will have a strong influence on salt ion partitioning and hence ion swelling pressure. When $pH << pK_{\mathrm{A}}$, the polymer is uncharged, $f \to 0$ and $\lambda \to 1$, and swelling takes on a minimum value determined by the mixing and elastic stresses. When $pH >> pK_{\mathrm{A}}$, all acid groups are ionized with $f \to 1$, and swelling is maximal with λ substantially greater than 1.

Figure 3.1a displays the effect of fraction ionized, f, on uniaxial swelling ratio $\alpha = \chi_1 = 0.48$, $\chi_2 = 0.60$. This figure was generated using equation (3.26) with $s = 0$ and a version of (3.24). As expected, swelling increases with decreasing salt concentration. For $C'_{\mathrm{NaCl}} = 250$mM, the membrane remains in its essentially collapsed state with $\alpha < 1$. In this case hydrophobicity is the dominant force, and the effect of ion osmotic stress is relatively weak. For $C'_{\mathrm{NaCl}} = 155$mM and 50mM, an initially shallow relation between α and f is punctuated by a rather sharp rise, indicating initial dominance of hydrophobicity that is overcome by ion osmotic stress at higher f. As ionic strength (salt concentration) decreases, the sharp rise occurs at lower ionization degree.

For $C'_{\mathrm{NaCl}} = 250$mM and 155mM, f uniquely determines α. For $C'_{\mathrm{NaCl}} = 50$mM, however, a range of bistability and hysteresis is observed. Over this range in f, total stress s vanishes at three values of α, corresponding to two free energy minima and one maximum in between. The latter, which corresponds to the negative slope branch of the swelling curve between the turning points, is unstable, and need not be considered in the discussion of equilibria. Figure 3.1b shows the fixed charge density, $\sigma = (\phi/\phi_0)f\sigma_0$, as a function of f for the three salt concentrations. In all cases, this quantity initially rises with increasing f, since f is increasing but swelling does not change significantly. The rise is followed by a drop attributed to the sudden increase in swelling. Bistability is observed for $C'_{\mathrm{NaCl}} = 50$mM over the same interval of f as before.

Figure 3.1c exhibits the calculated Donnan ratio λ as a function of f for the three salt concentrations. While these ratios provide information regarding the ion osmotic swelling force via (3.25), they also provide a link between external and internal pH. The curves are all nonmonotonic, with bistability for $C'_{\mathrm{NaCl}} = 50$mM. The swings in λ more or less follow those of σ and can be explained in essentially the same way.

Figure 3.2 displays the relationship between pH and swelling for the three salt concentrations, considering both internal and external pHs (dotted and continuous lines, respectively). These values are determined
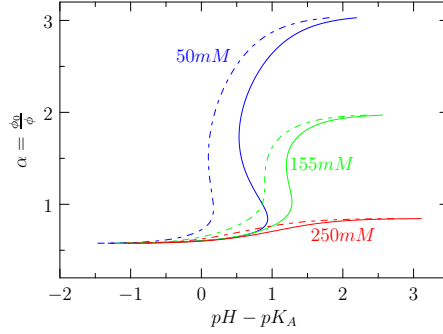
FIG. 3.2. *Swelling Ratio α versus $pH - pK_A$ at different salt concentrations.*

according to (3.24) and (3.26), with $s = 0$, and $pH(int) = -\log C_{\mathrm{H}}$ and $pH(ext) = pH(int) + \log \lambda$. Evidently, increasing salt concentration leads to an alkaline shift (higher pH) at which the major transition in swelling occurs. With increasing salt, a larger degree of ionization and hence higher pH is needed to effect the transition. The three pairs of graphs exhibit qualitatively different behaviors. For $C'_{\mathrm{NaCl}} = 250$mM, both curves are monotonic and single valued, although internal pH is clearly lower than external pH, as expected based on Donnan partitioning of hydrogen ion. For $C'_{\mathrm{NaCl}} = 50mM$, both curves exhibit bistability. At the intermediate salt concentration, $C'_{\mathrm{NaCl}} = 155$mM, the internal pH curve is single valued, while the external pH curve shows bistability. This difference can be attributed to the Donnan effect, which nudges external pH to higher values at low degrees of ionization and swelling. Of course, the real control variable is external pH.

We conclude that there are two potential mechanisms underlying bistability, one originating from the relation between fixed charge density and degree of swelling, and the other stemming from the Donnan effect. While in these studies we looked at qualitative behaviors as a function of C'_{NaCl}, these behaviors might also be observed by altering structural parameters of the hydrogel. To simplify the notation, from now on, we will remove the 'prime' symbol from the external salt concentration variable C'_{NaCl} and agree in writing C_{NaCl} instead.

4. Spatially homogeneous chemomechanical model. Now that the axially restricted equilibrium swelling properties of the hydrogel membrane have been explored, we introduce a lumped parameter model of the chemomechanical oscillator illustrated in Figure 1. Variants of this model have been presented previously [2, 9]. The dynamic model is based on the following assumptions:

a. Membrane properties, including the fixed charge concentration, swelling state and ion concentrations inside the membrane are assumed to be homogeneous in space. Upon suppressing lateral swelling and shrinking, the swelling state of the membrane is determined by its thickness $L = L(t)$. This homogeneity assumption is made even though the membrane is subjected to a pH gradient. External pH is "homogenized" by averaging the constant H^+ concentration in Cell I, C_H^I and the variable H^+ concentration in Cell II, C_H^{II}, that is, $pH = \log[(C_H^I + C_H^{II})/2]$.

b. Chemical potentials inside the membrane are determined by the 1-D FRDL equation of state for one-dimensional swelling, as described above. From these, the total swelling stress, including the elastic, mixing and ionic contributions, is given by (3.26), with λ determined according to the electroneutrality condition (3.24). Electroneutrality is enforced by rapid exchange of Na^+ and Cl^- between the membrane and Cells I and II. NaCl concentrations in Cells I and II are assumed constant and equal [18].

c. Enzymatic conversion of glucose to gluconic acid is assumed to be instantaneous. This assumption is valid when the concentration of enzyme in Cell II is sufficiently high that transport of glucose into Cell II is rate limiting. Also, gluconate and bicarbonate, produced according to chemical reactions (I) and (II), respectively, are presumed to not perturb the system's dynamics. The latter assumption is expected to hold best during early oscillations.

(d) The rate of change of fixed, negative charge concentration is controlled by the rate of transport of hydrogen ions, which reversibly bind to pendant carboxylates as they diffuse through the membrane [17].

(e) Permeability of the membrane to glucose is expressed as $K_{\mathrm{G}}^{\mathrm{o}} e^{-\beta\phi}$, as suggested by free volume theory [24], [35]. The parameters $K_{\mathrm{G}}^{\mathrm{o}}$ and β represent, respectively, the hypothetical permeability with vanishing

polymer concentration, and the sieving effect of the polymer, which depends on both polymer chain diameter and radius of the diffusant (glucose in this case). For hydrogen ions or water, which are much smaller than glucose, the sieving factor is assumed to be negligible, and we simply multiply the respective permeability coefficients, K_{h} and K_{w}, by $1 - \phi$ to account for the aqueous space in the hydrogel that is available for transport of solutes.

REMARK 2. *In this model, diffusion of Na^+ and Cl^- are regarded as instantaneous, while diffusion of H^+ is regarded as rate determining, even though the diffusion coefficient of H^+ is decidedly larger. This assumption is justified in part due to the reversible binding of H^+ to the pendant carboxylates, which does not occur with Na^+ and Cl^-, and partly due to the very low H^+ concentration, which qualifies it for "minority carrier" status. Changes in concentration of H^+ in the membrane are rapidly "buffered" by readjustments of Na^+ and Cl^- concentrations, preserving electroneutrality.*

Based on these assumptions, we write the following differential equations for L, the flux of hydrogen ions into the membrane, which then become either free intramembrane hydrogen ions or protons bound to pendant carboxyls, with respective concentrations C_{H} and C_{AH}, and the flux of H^+ to cell II:

$$\frac{dL}{dt} = -K_{\mathrm{w}}(1-\phi)[ln(1-\phi) + \phi + (\chi_1 + \chi_2\phi)\phi^2 + \nu_{\mathrm{w}}\rho_0(\frac{\phi_0}{\phi} - \frac{\phi}{2\phi_0})$$

$$-\nu_{\mathrm{w}}C_{\mathrm{NaCl}}(\lambda + \frac{1}{\lambda} - 2)], \tag{4.1}$$

$$\frac{d}{dt}[L(C_{\mathrm{H}} + C_{\mathrm{AH}})] = 2K_{\mathrm{h}}(1-\phi)[\lambda\frac{(C_{\mathrm{H}}^{\mathrm{I}} + C_{\mathrm{H}}^{\mathrm{II}})}{2} - C_{\mathrm{H}}], \tag{4.2}$$

$$\frac{d}{dt}C_{\mathrm{H}}^{\mathrm{II}} = \frac{AK_{\mathrm{G}}^0}{V}e^{-\beta\phi}C_{\mathrm{G}} - \frac{AK_{\mathrm{h}}}{V}(1-\phi)(\lambda C_{\mathrm{H}}^{\mathrm{II}} - C_{\mathrm{H}}) - k_{\mathrm{mar}}C_{\mathrm{H}}^{\mathrm{II}}, \tag{4.3}$$

where V is the volume of Cell II and C_{G} is the glucose concentration in Cell I. Then, the governing system consists of equations (4.1)-(4.3) together with the algebraic constraints (3.3), (3.18), (3.21) and (3.24). With an additional scaling argument, we obtain the equations to analyze.

5. Model scaling and the governing system. In this section, we identify the relevant parameters of the system and their numerical values. This will allow us to rigorously derive a reduced model from the system of equations (4.1)-(4.3). Five dimensionless groups give the system multiscale structure and properties, such as the role of the lower dimensional manifold discussed in section 7. However, the full dynamics cannot be explained in terms of the dimensionless parameter groups only. We find that the range of the oscillatory behavior is further determined by a few individual parameters, such as C_{NaCl}, σ_0 and ϕ_0, with the remaining ones held fixed. These values are in full agreement with the experiments and are also those used in the simulations of sections 3.4 and 6.

For convenience, we relabel the variable fields of the problem and define dimensionless variables:

$$x = C_{\mathrm{H}}, \ y = C_{\mathrm{AH}}, \ z = C_{\mathrm{H}}^{\mathrm{II}}, \ h = C_{\mathrm{H}}^{\mathrm{I}}, \tag{5.1}$$

$$\bar{x} = \frac{x}{c}, \quad \bar{y} = \frac{y}{c}, \quad \bar{z} = \frac{z}{c}, \quad \bar{L} = \frac{L}{L_0}, \quad \bar{t} = \frac{t}{T}, \tag{5.2}$$

where T and c are typical time and concentration variables, respectively. For now, we use the superimposed *bar* notation to represent dimensionless quantities. We choose

$$T = \frac{L_0\phi_0}{K_{\mathrm{w}}}, \quad c = K_{\mathrm{A}}. \tag{5.3}$$

Note that T corresponds to the time scale of equation (4.1), which will allow us to properly separate the dynamics of the membrane from that of the chemical reactions. The choice of c will lead to a reduced model resulting from the simplification of equation (4.2) as we shall see later in the section.

We now introduce five relevant dimensionless parameter groups consistent with the proposed scaling:

$$\mathcal{A}_1 = \frac{A}{V}\frac{C_{\mathrm{G}}}{K_{\mathrm{A}}}K_{\mathrm{G}}^0 T, \quad \mathcal{A}_2 = \frac{A}{V}TK_{\mathrm{H}}, \quad \mathcal{A}_3 = k_{\mathrm{mar}}T, \quad \mathcal{A}_4 = 2\frac{K_{\mathrm{H}}}{K_w}\phi_0\frac{K_{\mathrm{A}}\phi_0}{\sigma_0}, \quad \mathcal{A}_5 = \frac{K_{\mathrm{A}}\phi_0}{\sigma_0}. \tag{5.4}$$

The scaled form of equation (3.21) combined with (3.18) is then

$$\bar{y} = \mathcal{A}_5^{-1}\frac{\phi\bar{x}}{1+\bar{x}}, \quad \text{so} \quad \bar{x}+\bar{y} = \bar{x}(1+\mathcal{A}_5^{-1}\frac{\phi}{1+\bar{x}}) = \mathcal{A}_5^{-1}\frac{\bar{x}\phi}{1+\bar{x}} + O(1). \tag{5.5}$$

The latter approximation holds for the range of parameters of the problem, for which $\mathcal{A}_5^{-1} \approx 3*10^4$. Applying it to the scaled version of equation (4.2), which together with (4.1) and (4.3), give the set of equations of the model that we analyse:

$$\frac{d\phi}{d\bar{t}} = \mathcal{R}_1, \tag{5.6}$$

$$\frac{d\bar{x}}{d\bar{t}} = \mathcal{A}_4\mathcal{R}_2 + \mathcal{A}_5(1+\bar{x})^2\mathcal{R}_1, \tag{5.7}$$

$$\frac{d\bar{z}}{d\bar{t}} = \mathcal{A}_1\mathcal{R}_3, \tag{5.8}$$

$$\lambda = p(\phi)f + \sqrt{p^2(\phi)f^2 + 1}, \quad f = (1+\bar{x})^{-1}, \tag{5.9}$$

where

$$\mathcal{R}_1(\phi,\lambda) = (1-\phi)\phi^2\big(H(\phi) - R(\lambda)\big), \quad \mathcal{R}_2(\phi,x,\lambda) = (1-\phi)(1+x)^2(\frac{\lambda}{2}\bar{z} - \bar{x}), \tag{5.10}$$

$$\mathcal{R}_3(\phi,x,z,\lambda) = e^{-\beta\phi} - \mathcal{A}_2\mathcal{A}_1^{-1}(1-\phi)(\lambda\bar{z} - \bar{x}) - \mathcal{A}_3\mathcal{A}_1^{-1}\bar{z}, \quad \text{and} \tag{5.11}$$

$$H(\phi) = \ln(1-\phi) + \phi + (\chi_1 + \phi\chi_2)\phi^2 + \bar{\nu}_{\mathrm{w}}\bar{\rho}_0(\frac{\phi_0}{\phi} - \frac{\phi}{2\phi_0}), \tag{5.12}$$

$$R(\lambda) = \nu_{\mathrm{w}}C_{\mathrm{NaCl}}(\sqrt{\lambda} - \frac{1}{\sqrt{\lambda}})^2, \quad p(\phi) = \frac{\gamma\phi}{2(1-\phi)}, \tag{5.13}$$

$$q(\phi) = 1 + \frac{1}{2\gamma_0}H(\phi), \quad \gamma = \frac{\sigma_0}{C_{\mathrm{NaCl}}\phi_0}, \quad \gamma_0 = v_{\mathrm{w}}C_{\mathrm{NaCl}}. \tag{5.14}$$

The graph of $H(\phi)$ is shown in figure 5.1.

Parameters of the problem, shown in tables (S2)-(S4) of the Supplementary Materials section, are of three main types: device specifications, hydrogel parameters and rate quantities. It should be noted that while some of these values either reflect the experimental conditions or are literature parameters for NIPA/MAA hydrogels [27], some parameters were chosen to produce results that are in line with experimental observations. Specifically, the size of the marble component in Cell II was chosen with a sufficiently large surface area so as to provide the necessary reaction sites to remove excessive hydrogen ions from the system. For the given parameter values, we find that

$$\mathcal{A}_1 \approx 0.16*10^1, \ \mathcal{A}_2 \approx 0.52*10^{-2}, \ \mathcal{A}_3 \approx 0.75*10^{-2}, \ \mathcal{A}_4 \approx 0.33*10^{-5}. \tag{5.15}$$

We point out that $0 < \mathcal{A}_4 << 1$, $\mathcal{A}_1^0 := A_1e^{-\beta\phi_0} = 0.016$ and $\mathcal{A}_1^0 > \mathcal{A}_2, \mathcal{A}_3$. So, the first term of the right hand side of (5.8) is of the order $\mathcal{A}_1^0$, since

$$\mathcal{A}_1\mathcal{R}_3 = \mathcal{A}_1^0e^{-\beta(\phi-\phi_0)} + \ldots \tag{5.16}$$

These parameter properties are relevant to obtain estimates of the solutions.

DEFINITION 5.1. *We let $\mathcal{P}$ denote the set of parameters in tables (S2)-(S4) and with*

$$C_{NaCl} \in [20*10^{-3}, 155*10^{-3}]M, \quad \sigma_0 = [0.10, 0.40], \quad \phi_0 = [0.1, 0.3]. \tag{5.17}$$

Experiments have been carried out with values of C_{NaCl} in the list $\{350, 250, 150, 100, 50, 40, 25, 20\} * 10^{-3}$M. However for salt concentration values above $155*10^{-3}$M, no oscillatory behaviour has been found.

From now on, we suppress the superimposed *bar* in the equations and assume that all variables are scaled. We now study the properties of the functions in the governing system.

LEMMA 5.2. *Suppose that the parameters in (5.12) belong to $\mathcal{P}$. Then the function $H(\phi)$ is non-monotonic in $(0,1)$ and has the following properties:*

$$\lim_{\phi\to0^+} H(\phi) = \infty, \quad H(\phi) = O(\frac{1}{\phi}) \ \text{and} \ \lim_{\phi\to1^-} H(\phi) = -\infty, \quad H(\phi) = O(\log(1-\phi)). \tag{5.18}$$
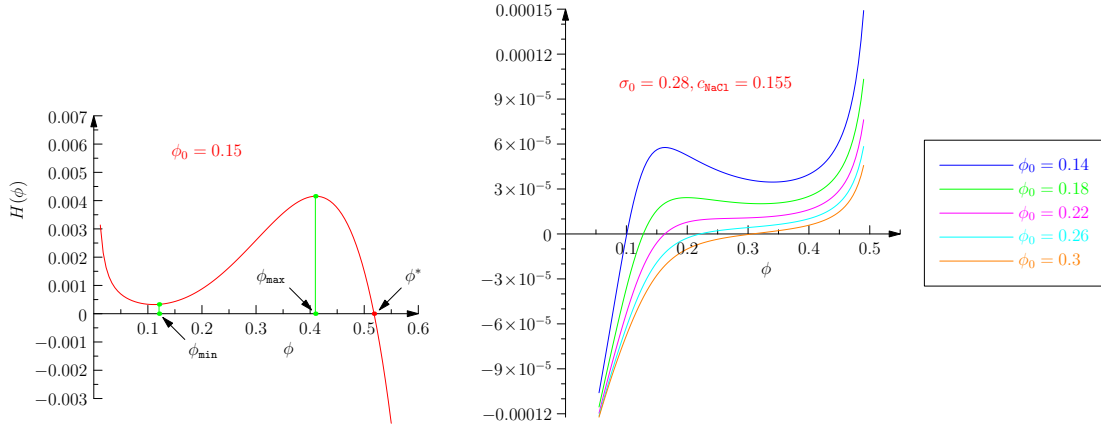
FIG. 5.1. *(Left) Plot of the mechanical compliance $H(\phi)$ for parameters values: $\chi_1 = .48, \chi_2 = .6$ and $\phi_0 = .3$; $\phi^* = 0.5226$. (Right) Plot of the left hand side function of equation (6.1)*

Moreover, there exists a unique $\phi^* \in (0,1)$ such that $H(\phi^*) = 0$. Furthermore, $H(\phi)$ has a unique local maximum, ϕ_{max} and a unique local minimum, ϕ_{min} in $(0, \phi^*)$, as shown in Figure 5.

We represent the governing system (5.6)-(5.8) and denote the corresponding domain as

$$\dot{\mathbf{x}} = \boldsymbol{f}(\mathbf{x}) \quad \text{and} \quad \mathcal{I} = \{\mathbf{x} = (\phi, x, z) : \phi \in (0,1), x \in (0,\infty), z \in (0,\infty)\}, \tag{5.19}$$

respectively, with the components of $\boldsymbol{f}$ given by the right hand side functions of the system. It is easy to check that $\boldsymbol{f}$ is continuously differentiable in the convex set $\mathcal{I}$, also the set of initial data of the problem. In order to denote solutions corresponding to specific initial data in $\mathcal{I}$, we write

$$\phi(t) = \phi(\phi^0, x^0, z^0)(t), \ x(t) = x(\phi^0, x^0, z^0)(t), \ z(t) = z(\phi^0, x^0, z^0)(t),$$
$$\phi_M(t) = \phi(\phi^0, x^+(\phi^0), z^0)(t), \ x(t) = x(\phi^0, x^+(\phi^0), z^0)(t), \ z(t) = z(\phi^0, x^+(\phi^0), z^0)(t),$$

with the latter expression referring to restrictions to the two-dimensional manifold $\mathcal{M}$ defined in (7.8).

5.0.1. Time scales of the model. The relative sizes of the dimensionless parameters $\mathcal{A}_i$, in particular, the fact that $\mathcal{A}_4 << 1$ in equation (5.7) indicates that x is the slow field of the problem. Accordingly, we define the time scale associated with x as

$$\tau = \mathcal{A}_4 \bar{t} = \frac{\mathcal{A}_4}{T} t, \quad \epsilon := \mathcal{A}_4, \quad \mu = \frac{\mathcal{A}_4}{\mathcal{A}_1}. \tag{5.20}$$

So, the original dimensionless time variable $\bar{t}$ corresponds to the *fast* dynamics, whereas τ gives the *slow* time, that now we take as reference. In the new time scale, the governing system reduces to

$$\mathcal{A}_4 \frac{d\phi}{d\tau} = \mathcal{R}_1(\phi, \lambda) \tag{5.21}$$

$$\frac{d\bar{x}}{d\tau} = \mathcal{R}_2(\phi, \bar{x}, \lambda) + \frac{K_A \phi_0}{\sigma_0 \mathcal{A}_4}(1 + \bar{x})^2 \mathcal{R}_1, \tag{5.22}$$

$$\frac{\mathcal{A}_4}{\mathcal{A}_1} \frac{d\bar{z}}{d\tau} = \mathcal{R}_3(\phi, \bar{x}, \bar{z}, \lambda), \tag{5.23}$$

together with equations (5.9). For our typical parameter values, $\mathcal{A}_4 = 0.33 * 10^{-5}$, $\frac{\mathcal{A}_4}{\mathcal{A}_1^0} = 0.12 * 10^{-3}$ and $\frac{K_A \phi_0}{\mathcal{A}_4 \sigma_0} = 10$. This motivates identifying a reduced model consisting of equations (5.22)-(5.23) together with the algebraic equation $0 = \mathcal{R}_1(\phi, \lambda)$, and equations (5.9). We also point out that the scaling falls through when $\phi > 0$ is arbitrarily small, that is, for highly swollen regimes. This follows from estimating equation (5.6) for $\phi > 0$ small as well as the observation that $\lambda = O(1)$ and $R(\lambda) \approx 0$. Specifically, for given $\varepsilon > 0$, and for $\phi \in (0, \varepsilon)$:

$$p(\phi) = \gamma\phi + o(\varepsilon), \quad \lambda = 1 + o(\varepsilon), \quad R(\lambda) = o(\varepsilon), \quad H(\phi) = v_{\text{w}}\rho_0 \frac{\phi_0}{\phi} + o(\varepsilon). \tag{5.24}$$

This allows us to establish the following lemma:

LEMMA 5.3. *Let $\tilde{T} > 0$ be such that $\phi = \phi(t)$ and $\lambda = \lambda(t)$ satisfy equation (5.6) for $t \in [0, \tilde{T}]$. Then*

$$\frac{d\phi}{dt} = \frac{\nu_w \rho_0}{\mathcal{A}_4} O(\frac{1}{\phi}) \ as \ \phi \to 0^+. \tag{5.25}$$

The behavior of the constitutive functions in (5.24) yields the following:

PROPOSITION 5.4. *Solutions of (5.6) corresponding to initial data in $\mathcal{I}$ have the property that ϕ remains bounded away from $\phi = 0$ and $\phi = 1$ for all time. Moreover, there exist positive numbers t_m and t_M, depending on the initial data, such that $\phi(t_m) > 0$ and $\phi(t_M) > 0$ are minimum and maximum values of ϕ, respectively.*

Proof. Let us first recall that ϕ^* denotes the largest value of ϕ such that $H(\phi^*) = 0$. From the governing equation for ϕ, we see that for initial data $\phi_i \geq \phi^*$, $\frac{d\phi}{dt} < 0$. This proves the boundedness of the orbit away from $\phi = 1$. Let us consider an orbit with initial data $\phi_i \in (0, \epsilon)$ and such that $\frac{d\phi}{dt} < 0$ at some $t > 0$. Integrating the governing equation for ϕ while taking into account the estimates in (5.24) on its right hand side function yields $\phi(t) = \phi_i O(e^{\frac{t}{\nu_w \rho_0 \phi_0}})$. This contradicts the assumption that $\frac{d\phi}{dt} < 0$ at some $t > 0$, and so proving the statement of the proposition. $\square$

REMARK 3. *Proposition (5.4) states that the solution ϕ of the governing system remains in the interval $(0, 1)$, for all time of existence. However, due to the separation of time scales, only disconnected subintervals of $(0, 1)$ are admissible. This is the topic of the next section.*

The following lemma is used in the estimate of bounds of solutions. Let us rewrite equation (5.8) as

$$\frac{dz}{dt} + w(t)z = g(t) \ \text{with} \ w := \mathcal{A}_2(\lambda(1 - \phi) + 1), \quad g := \mathcal{A}_1 e^{-\beta\phi} + \mathcal{A}_2(1 - \phi)x. \tag{5.26}$$

The proof follows by integration of the previous auxiliary equation.

LEMMA 5.5. *Suppose that $z_0 > 0$, $x = x(t)$, $\phi = \phi(t)$ and $\lambda = \lambda(t)$ are prescribed, continuous functions with $t \in [0, \hat{T}]$, for some $\hat{T} > 0$. Then, the solution of (5.8) satisfies the equation*

$$z(t) = E^{-1}(t)\Big(z_0 + \int_0^t E(s)g(s)\,ds\Big), \ t \in [0, \hat{T}], \ z_0 = z(0), \quad \text{and} \ E(t) := \exp\int_0^t w(s)\,ds. \tag{5.27}$$

Next, we show that solutions of (5.7) remain bounded away from $x = 0$.

LEMMA 5.6. *Suppose that $\phi = \phi(t)$ and $z = z(t) > 0$ are prescribed continuous functions for $t \geq 0$, and such that $\phi(t)$ and $z(t)$ remain bounded away from $\phi = 0$ and $z = 0$, respectively. Then the solution $x = x(t)$ of equation (5.7) corresponding to initial data $x(0) > 0$ remains bounded away from $x = 0$ for all $t > 0$.*

Proof. We argue by contradiction and assume that for a prescribed arbitrarily small $\epsilon > 0$, there exits $t_1 = t_1(\epsilon) > 0$ such that $0 \leq x(t) \leq x(t_1) \leq \varepsilon$, for $t \geq t_1$. A simple calculation using (5.9) gives

$$\lambda(t_1) = p(\phi(t_1)) + \sqrt{p^2(\phi(t_1)) + 1} + O(\varepsilon). \tag{5.28}$$

Hence, $\mathcal{R}_2(t_1) \geq (1 - \phi(t_1))(1 + x(t_1))^2(\frac{\lambda(t_1)}{2}z(t_1) - \varepsilon)$. So, $\frac{dx}{dt}(t_1) > 0$ and bounded away from 0, and therefore, $x(t)$ cannot further decrease to 0. $\square$

Using the previous lemmas on boundedness of solutions, we can now state the following.

PROPOSITION 5.7. *Suppose that the parameters of the governing system belong to $\mathcal{P}$. Let $\{\phi = \phi(t), x = x(t), z = z(t)\}$, $t \in [0, T)$, denote a solution of the system (5.6)-(5.8) and (5.9) corresponding to initial data in $\mathcal{I}$, and with $T > 0$ representing the maximal time of existence. Then $\{\phi(t), x(t), z(t)\}$ are bounded. Moreover, the lower bounds are strictly positive and the upper bound of ϕ is strictly less than 1. Furthermore, $\mathcal{I}$ is invariant under the flow of the governing system.*

6. Hopf bifurcation: a numerical study. We numerically investigate the following properties of the solutions corresponding to the parameter set $\mathcal{P}$:

1. Uniqueness of the steady state solution and its stability.
2. Occurrence of Hopf bifurcation.
3. Non-monotonicity of the graph $x = x^+(\phi)$ in (7.6) and the reduced system (section (7)).
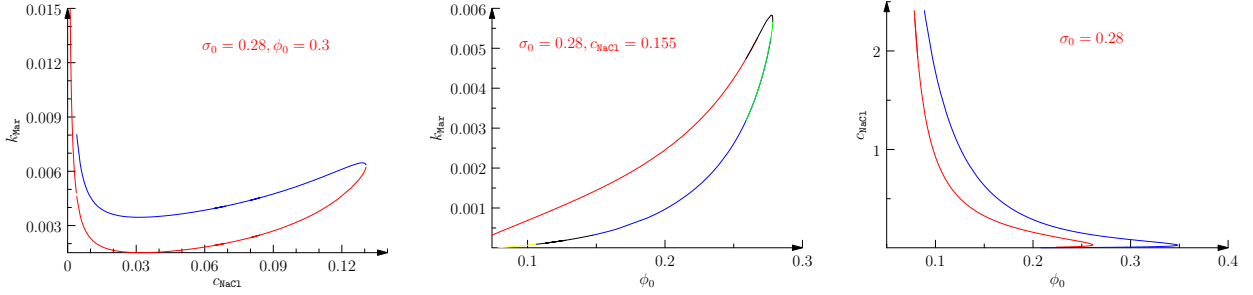
FIG. 6.1. *Hopf bifurcation diagrams in different parameter planes. The red line denotes the instability threshold.*

We have seen that the third property guarantees the construction of closed orbits of the approximate two-dimensional system. This together with existence of a unique, unstable steady state provide sufficient conditions for the Poincare-Bendixon theorem to apply, from which existence of a limit cycle follows.

Steady state values of the variables x, z and ϕ satisfy

$$x = \frac{\lambda}{2} z, \quad z = \mathcal{A}_1 e^{-\beta\phi}(\mathcal{A}_2(1-\phi)\frac{\lambda}{2} + \mathcal{A}_3)^{-1},$$
$$\frac{p}{\sqrt{q^2-1}} - 1 - \frac{\mathcal{A}_1}{2}\lambda e^{-\beta\phi}(\mathcal{A}_2(1-\phi)\frac{\lambda}{2} + \mathcal{A}_3)^{-1} = 0, \tag{6.1}$$

where the last equation follows from the previous expressions of x and z, together with relations (7.6) and (5.14). The second graph in Figure 5 shows plots of the function on the left hand side of equation (6.1) with the corresponding unique root, which after substitution into equations for x and z, yields their steady state values. The computational results summarized next are in full agreement with those of laboratory experiments.

1. For $C_{\mathrm{NaCl}} = 0.155$ M:

a. We found that for each $\phi_0 = 0.1, 0.15, 0.2, 0.295$, there is a unique physically relevant steady state, that is, with $\phi < \phi^*$. We point out that this result is valid for $\phi_0 \in [0.1, 0.3]$. This is justified by the implicit function theorem applied to the left hand side function in (6.1) with respect to each root. In this proof, we also use the fact that the slope of the tangent line to the graph at the intersection with the ϕ-axis is non-horizontal, as shown in figure 5 (Right).

b. The stability of the unique equilibrium solution is represented in the diagrams of figures 6.1. We find a region in parameters plane determined by the Hopf bifurcation curves, within which the equilibrium is unstable; outside, the solution is stable. The unstable equilibrium has a pair of complex conjugate eigenvalues with positive real part and a negative eigenvalue. Consequently, the existence of a Hopf bifurcation is guaranteed by the *Hopf bifurcation theorem* [19] (section 3).

c. The graph $x = x(\phi)$ of the function (7.6) is found to be non-monotonic inside the regions determined by the Hopf bifurcation curves in figures 6.1 and monotonic outside. Oscillatory behaviour is numerically found inside these regions.

2. We have also found that decreasing C_{NaCl} gives a qualitative behavior analogous to decreasing ϕ_0, that is, it promotes a single unstable stationary state of the system and the occurrence of Hopf bifurcation. In particular, the following behaviors have been found:

a. For $C_{\mathrm{NaCl}} = 0.145$M and $\phi_0 = 0.3$, the steady state solution corresponds to $\phi = 0.145$.

b. For $C_{\mathrm{NaCl}} = 0.148$M and $\phi_0 = 0.3$, the maximum and minimum values of $x = x(s)$ occur at $\phi = 0.24$ and $\phi = 0.26$. In both, these cases, a Hopf bifurcation has also been found.

c. Hopf bifurcations have also been found for $C_{\mathrm{NaCl}} = 0.125$M and $C_{\mathrm{NaCl}} = 0.115$M.

d. For $\phi_0 = 0.3$, $C_{\mathrm{NaCl}} = 0.155$M and $\sigma_0 = 0.28$, no Hopf bifurcation occurs. The simulations do not show oscillatory behaviour and there is at least one stable stationary state.

7. Inertial manifold of the governing system. We now derive and study a reduced two-dimensional system such that, solutions of initial value problems of the original three-dimensional system remain arbitrarily close to those of reduced one, for most of the time of existence. Moreover, we shall see that, for the parameters of interest, the functions defining the 2-dimensional system are specified in two separate branches. So, it is

necessary to extend the concept of solution giving it a weak interpretation as shown in the next section. Weak solutions also give a good physical description of the phase transition features of the model.

In order to identify the slow manifold, we consider the nullcline

$$H(\phi) = R(\lambda) \tag{7.1}$$

of the original system. This corresponds to setting $\epsilon = 0$ in (5.21), so that $\mathcal{R}_1 \equiv 0$ while keeping μ fixed. Note that the right hand side of equation (5.22) is simplified accordingly.

We now list the properties of the solutions of the equation (7.1) that follow from the positivity of $R(\cdot)$ and the fact that $\lambda \geq 1$.

LEMMA 7.1. Let $H(\phi)$ and $R(\lambda)$ be as above. Then, solution pairs (ϕ, λ) of equation (7.1) satisfy:

$$0 < \phi \leq \phi^* \text{ so that } H(\phi) \geq 0 \quad \text{and} \quad \lambda > 1, \text{ with } \lambda = 1 \text{ when } \phi = \phi^*.$$

This allows us to characterize the nullcline (7.1) as

$$\mathcal{N} = \{(\phi, \lambda, z) \in \mathbf{R}^3 : 0 < \phi < 1, z > 0, \lambda > 1, H(\phi) = R(\lambda), \text{ and such that (5.9) holds}\}, \tag{7.2}$$

$$\mathcal{N} := \mathcal{N}^+ \cup \mathcal{N}^-, \quad \mathcal{N}^+ = \{(\phi, \lambda, z) \in \mathcal{N} : H'(\phi) > 0\}, \quad \mathcal{N}^- = \{(\phi, \lambda, z) \in \mathcal{N} : H'(\phi) \leq 0\}. \tag{7.3}$$

Since relations (5.9) define λ as a monotonic function of x, we can exchange the roles of x and λ in (7.2)-(7.3) at convenience.

Let us obtain an explicit representation of $\mathcal{N}$ and the governing equations of the reduced system. For this, we first solve equations (5.9) and (7.1) using (5.12) and (5.13) and (5.14) as follows

$$\frac{\gamma \phi}{(1 - \phi)} f = \lambda - \frac{1}{\lambda}, \quad \frac{H(\phi)}{\gamma_0} = \lambda + \frac{1}{\lambda} - 2. \tag{7.4}$$

Addition and subtraction of these equations yields

$$\lambda = q(\phi) + p(\phi)f, \quad \frac{1}{\lambda} = q(\phi) - p(\phi)f, \tag{7.5}$$

respectively, which, in turn, give the equation $f_+ = \frac{1}{p}\sqrt{q^2 - 1}$, for $q \geq 1$ and with $H(\phi) \geq 0$. The corresponding values of the concentration x and the Donnan ratio λ are

$$x^+ = \frac{p(\phi)}{\sqrt{q^2(\phi) - 1}} - 1, \quad \lambda^+ = q(\phi) + \sqrt{q^2(\phi) - 1}, \tag{7.6}$$

respectively. Figures 7.1 present the graphs of these functions, for parameters in the class $\mathcal{P}$, showing their non-monotonicity. We label the critical points of $x^+(\phi)$ as

$$0 < \phi_s^1 < \phi_s^2 : \frac{dx^+}{d\phi}(\phi_s^i) = 0, \ i = 1, 2, \quad \text{and} \quad x_s^i := x^+(\phi_s^i), \tag{7.7}$$

and consider the strictly increasing branches $(0, \phi_s^1) \cup (\phi_s^2, \phi^*)$. Let $\phi^+(x)$ denote the inverse of the restrictions of $x^+(\phi)$ to the monotonic branches, and define

$$\mathcal{M}_1 := \{(\phi, x, z) : z \geq 0, x = x^+(\phi), \phi \in (0, \phi_s^1)\}, \quad \mathcal{M}_2 := \{(\phi, x, z) : z \geq 0, x = x^+(\phi), \phi \in (\phi_s^2, \phi^*)\},$$

$$\mathcal{M} := \mathcal{M}_1 \cup \mathcal{M}_2, \quad \mathcal{M}^- := \{(\phi, x, z) : z \geq 0, x = x^+(\phi), \phi \in (\phi_s^1, \phi_s^2)\}. \tag{7.8}$$

That is, $\mathcal{M}$ consists of two branches where $x^+(\phi)$ increases monotonically. We point out that this graph is the cross section with respect to z of the surface $H(\phi) = R(\lambda)$. This surface divides the whole space into upper and lower regions, with $\mathcal{R}_1 > 0$ and $\mathcal{R}_1 < 0$, respectively.

We now study the governing system restricted to $\mathcal{M}$. In terms of the original dimensionless time variable (which we still denote by t) and dependent variables, the governing system in $\mathcal{M}$ reduces to

$$\frac{dx}{dt} = \mathcal{A}_4 \phi (1 - \phi)(1 + \gamma \phi f^2)^{-1} \left(\frac{\lambda}{2} z - x\right), \quad \frac{dz}{dt} = \mathcal{A}_1 e^{-\beta \phi} - \mathcal{A}_2 (1 - \phi)(\lambda z - x) - \mathcal{A}_3 z, \tag{7.9}$$
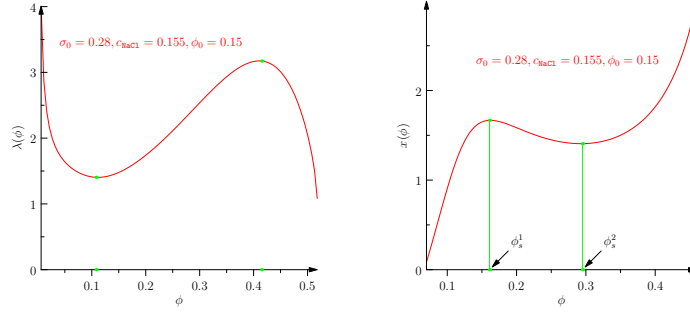
FIG. 7.1. *Plot of $\lambda = \lambda^+(\phi)$ and $x = x^+(\phi)$ from equations (7.6) that enter in the definition of $\mathcal{M}$*

together with equations (7.6).

PROPOSITION 7.2. *Suppose that the parameters of the problem belong to the class $\mathcal{P}$. Then $\mathcal{M} \cup \mathcal{M}^-$ is a two-dimensional invariant manifold of the three-dimensional system. Furthermore, the vector field of the two dimensional system is Lipschitz in $\mathcal{M}$. Moreover, $\mathcal{N}^- \subset \mathcal{M}$.*

Proof. Let us consider initial data $(\phi_0, x_0, z_0) \in \mathcal{M} \cup \mathcal{M}^-$. It is easy to see that we can construct a solution of the three dimensional system belonging to $\mathcal{M} \cup \mathcal{M}^-$. So, by uniqueness, solutions with initial data satisfying $x_0 = x^+(\phi_0)$, $\phi_0 \in (0, \phi^*)$ belong to $\mathcal{M} \cup \mathcal{M}^-$, for all time of existence. Moreover, applying the same arguments as in Proposition 5.7, we find that $x(t)$ remains bounded away from $x = 0$, and so $\phi(t) > \phi^{**}$, for all $t > 0$. The last statement of the proposition follows by taking the derivative with respect to ϕ of the function $x = x^+(\phi)$ in equation (7.6), to give

$$\frac{dx}{d\phi} = \frac{1}{\sqrt{q^2 - 1}}\left((1-\phi)^{-2} - \frac{pq}{q^2-1}H'(\phi)\right). \tag{7.10}$$

So, $H'(\phi) < 0$ implies that $\frac{dx}{d\phi} > 0$, for $\phi < \phi^*$. $\square$

In order to study solutions with initial data outside $\mathcal{M} \cup \mathcal{M}^-$, we observe the following properties of the term $\mathcal{R}_1$:

$$\mathcal{R}_1 > 0 \text{ for } x > x^+(\phi) \quad \text{and} \quad \mathcal{R}_1 < 0 \text{ for } x < x^+(\phi). \tag{7.11}$$

PROPOSITION 7.3. *Suppose that the parameters of the system belong to the class $\mathcal{P}$. Then the following statements on the three-dimensional system hold:*

1. *Solutions with initial data such that $x^0 \neq x^+(\phi^0)$ have the property that $|\mathcal{R}_1(\phi(t), x(t))|$ decreases with respect to t, for sufficiently large $t > 0$. In particular, $|\mathcal{R}_1|$ is strictly decreasing for $\phi^0 \in (0, \phi_s^1) \cup (\phi_s^2, \phi^*)$, for all $t > 0$.*
2. *Let $\epsilon > 0$ be sufficiently small. Then $\mathcal{M}$ is asymptotically stable, that is, there exists $(\hat{\phi}(t), \hat{x}(t), \hat{z}(t)) \in \mathcal{M}$ such that, for sufficiently large t, solutions corresponding to initial data $(\phi^0, x^0, z^0) \in \mathcal{I}$ satisfy*

$$\phi(t, \epsilon) = \hat{\phi}(t) + O(e^{-\frac{t}{\epsilon}}), \ x(t, \epsilon) = \hat{x}(t) + O(e^{-\frac{t}{\epsilon}}), \ z(t, \epsilon) = \hat{z}(t) + O(e^{-\frac{t}{\epsilon}}). \tag{7.12}$$

Proof. Part 1 follows directly from the first equation in (5.10), the properties of the functions $H(\phi)$ and $R(\lambda)$ and (5.6). The functions $(\hat{\phi}(t), \hat{x}(t), \hat{z}(t))$ are obtained as weak solutions of the two dimensional system. Their construction applies Definition 7.4, and estimate (7.12) follows from Theorem 9.2 on multiscale analysis of the system. $\square$

We characterize weak solutions of the two dimensional system. These correspond to hysteresis loops on the left graph of figure 5.1. One main ingredient in the construction is the theorem on continuation and finite time blow-up of solutions of ordinary differential equations together with the existence of unique, unstable, equilibrium point. This, together with the Poincaré-Bendixon theorem for two dimensional systems, leads to the existence of a limit cycle for such a system. The latter is also the ω-limit set of the positive semi-orbits of the three dimensional system.

DEFINITION 7.4. *A weak solution of the two dimensional system corresponding to initial data $(\phi^0, x^0, z^0) \in \mathcal{M}$ has the following properties:*

1. *There exists $0 < \hat{t}$ such that $(\phi(t), x(t), z(t))$ is a classical solution for $t \in (0, \hat{t})$.*
2. *$\phi(\hat{t}) = \phi_s^1$ (or ϕ_s^2).*
3. *$\phi(t)$ is discontinuous at $\hat{t}$ experiencing a jump $[\phi(\hat{t})] = \phi_s^2 - \phi_s^1$. (alternatively, $[\phi(\hat{t})] = \phi_s^1 - \phi_s^2$.)*
4. *The time derivatives of ϕ experience finite time blow up, that is, $\lim_{t \to \hat{t}} \frac{d\phi}{dt}(t) = +\infty$ (alternatively,*
   $\lim_{t \to \hat{t}} \frac{d\phi}{dt}(t) = -\infty$).
5. *$x(t)$ and $z(t)$ are continuous at $\hat{t}$ and their derivatives experience a jump discontinuity.*
6. *The solutions can be continued for $t > \hat{t}$ and are bounded.*

REMARK 4. *We point out that $\mathcal{M}^-$ is also an invariant manifold of the two-dimensional system. In particular, it contains the unique stationary point, with eigenvalues forming a complex conjugate pair, with positive real part. The limit cycle of the 2 dimensional system found next is also the ω-limit set of solutions with initial data in $\mathcal{M}^-$.*

We point out that values of $\phi \in (\phi_s^1, \phi_s^2)$ are excluded from the range of solutions of the two-dimensional system. Indeed, in the next section, we construct weak solutions of the system such that ϕ experiences jump discontinuities, so as to avoid this interval. However, this interval is accessible to solutions of the full system, and, in particular, it contains the unique unstable equilibrium point. We will also show that this interval is covered in the fast time scale. The following result follows from the uniqueness of classical solutions of the initial value problem of the system (5.6)-(5.13).

We denote the weak solution as $\boldsymbol{\psi}_{\mathcal{M},t} = (\phi_\mathcal{M}, x_\mathcal{M}(\phi), z_\mathcal{M})$, where $\boldsymbol{\psi}_{\mathcal{M},t}$ is the flow. Let $\boldsymbol{\varphi}_t$ denote the flow of the three dimensional system with initial data in $\mathcal{I}$.

THEOREM 7.5. *For each set of initial data $(\phi^0, x^0, z^0) \in \mathcal{M}$, there is a a unique weak solution $(\phi_\mathcal{M}(t), x_\mathcal{M}(t), z_\mathcal{M}(t))$ of the two dimensional system, that exists for all $t > 0$. Moreover, the ω-limit set $\omega(\pi^+)$ of a semi-orbit π^+ of the three dimensional system with initial data in $\mathcal{I}$ satisfies $\omega(\pi^+) = \omega(\pi^+_\mathcal{M})$, where $\omega(\pi^+_\mathcal{M})$ is the ω-limit set of the trajectories of the two dimensional system.*

Proof. Without loss of generality let us assume that $(\phi(0), x(0), z(0)) \in \mathcal{M}_2$ and with $\frac{1}{2}\lambda(x(0), \phi(0))z(0) - x(0) < 0$. Then, there is $\hat{t} > 0$ such that $(0, \hat{t})$ gives the maximal interval of existence of the classical solution of the 2-dimensional system. Two different situations may occur, according to the choice of initial data:

1. $\hat{t} = \infty$ in which case the solution is bounded and such that $x(t) \in \mathcal{M}_2$ for all time, or
2. $0 < \hat{t} < \infty$, in which case $x(\hat{t}) = x_s^2$, and $\phi(\hat{t}) = \phi_s^2$.

In case (2), we further distinguish two cases, also according to initial data:

2a. $\frac{1}{2}\lambda(x(\hat{t}), \phi(\hat{t}))z(t) - x(\hat{t}) = 0$, in which case $\frac{dx}{dt}(\hat{t}) = 0$. The solution can then be continued as in case 1, that is, as classical solution in $\mathcal{M}_2$, and, so it never reaches $\mathcal{M}_1$.

2b. $\frac{1}{2}\lambda(x(\hat{t}), \phi(\hat{t}))z(t) - x(\hat{t}) < 0$, and so $\frac{dx}{dt}(\hat{t}) < 0$. Since $\lim_{t \to \hat{t}} \frac{dx}{dt}(t) = 0$, then $\lim_{t \to \hat{t}} \frac{d\phi}{dt}(t) = -\infty$. We set $\phi(\hat{t}^+) = \phi_s^1$, so the jump condition $[\phi] = \phi_s^1 - \phi_s^2$ is satisfied, $x(\hat{t}^-) = x(\hat{t}^+) = x_s^2$ and $z(\hat{t}^-) = z(\hat{t}^+)$. Note that at $t = \hat{t}^+$, $(\phi, x, z) \in \mathcal{M}_1$.

To continue the solution for $t > \hat{t}$, we solve the initial value problem with initial data $(\phi(\hat{t}^+), x(\hat{t}^+), z(\hat{t}^+))$. It is easy to see that there is a time $\tilde{t} > \hat{t}$ such that $\lim_{t \to \tilde{t}^-} \phi(t) = \phi_s^1$ and $\lim_{t \to \tilde{t}^-} x(t) = x_s^1$. In fact, it follows from the fact that ϕ and x remain bounded away from 0, so that the values ϕ_s^1 and x_s^1, respectively, can be reached, allowing the solution to be continued in $\mathcal{M}_2$. The fact that $\phi < \phi^*$ and that there are no equilibrium points in $\mathcal{M}_2$ guarantees the existence of a point of return on the trajectory $(\phi(t), x(t), z(t))$, and so the process can be continued.

Since the orbits π^+ and $\pi^+_\mathcal{M}$ are both bounded, the scaling with respect to $\mathcal{A}_4$ holds and so does the estimate

$$|\phi(t) - \phi_\mathcal{M}(t)| = O(e^{-\frac{t}{\epsilon}}), \tag{7.13}$$

together with the analogous estimates for $x(t), z(t)$ which completes the proof of the theorem. $\square$

Since $\mathcal{M}$ is an invariant set that does not contain equilibrium points, the existence of a limit cycle for the two dimensional system follows from the Poincaré-Bendixon theorem stated next. Its corollary gives the stability of the limit cycle with respect to, both, the two-dimensional and the three-dimensional dynamics.

THEOREM 7.6 (Poincaré-Bendixon[20]). *If π^+ is a bounded semiorbit and $\omega(\pi^+)$ does not contain any critical point, then either $\pi^+ = \omega(\pi^+)$, or $\omega(\pi^+) = \bar{\pi}^+/\pi^+$. In either case, the $\omega - limit$ set is a periodic orbit. Moreover, for a periodic orbit π^0 to be asymptotically stable it is necessary and sufficient that there is a neighborhood G of π^0 such that $\omega(\pi(p)) = \pi^0$ for any $p \in G$.*
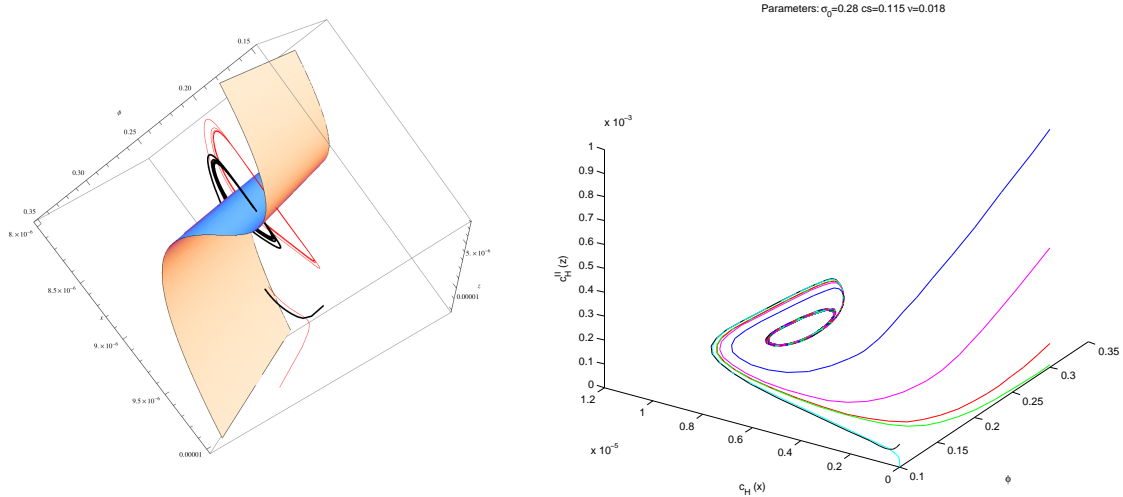
Parameters: σ_ϕ=0.28 cs=0.115 v=0.018

FIG. 7.2. *The left figure shows orbits of the three dimensional system with the manifold $\mathcal{M}$. The figure on the right shows plots of orbits of the three dimensional system approaching a plane closed curve. It is the ω-limit set of both systems and the limit cycle of the two dimensional system in the manifold $\mathcal{M}$.*

REMARK 5. *The orbits of the two-dimensional system analyzed in this section, and in particular the limit cycle, correspond to the projection to the $x - z$ plane of the three-dimensional orbits shown in figure 7.2(b). Moreover, these two-dimensional orbits correspond to the leading terms in expansions (9.2)-(9.3).* Next theorem shows that the limit cycle of the two dimensional system is also the limit cycle of the three dimensional one.

THEOREM 7.7. *Suppose that the parameters of the system belong to the class $\mathcal{P}$. Then the two-dimensional system has an asymptotically stable limit cycle π^+ in $\mathcal{M}$. Moreover π^+ is also the ω-limit set of positive semi-orbits of the three-dimensional system with initial data in $\mathcal{I}$.*

Proof. Let us consider solutions with initial data in $\mathcal{M}$. For these initial data, we previously showed that the two-dimensional system admits bounded weak solutions that exist for all time. Moreover, the orbits of these solutions do not contain any equilibrium point. So, the existence of a limit cycle π^+ in $\mathcal{M}$ follows directly from the Poincarè-Bendixon theorem. The asymptotic stability of π^+ follows from the boundedness of solutions and the absence of a stationary state in $\mathcal{M}$. To prove the last statement, let us consider solutions with initial data $(\phi^0, x^0, z^0) \in \mathcal{I}$ and such that $x^0 \neq x^+(\phi^0)$. By an estimate as (7.13), we can assert that sufficiently large t, $|x(t) - x_M(t)| = O(e^{-Mt})$, with $M > 0$ as in (9.4), and $x_M(t) := x_M(\phi^0, x^+(\phi^0), z^0)(t)$. This indicates that the solution of the three dimensional system approaches the two-dimensional manifold, for sufficiently large t. Since the only equilibrium point in the three-dimensional space is unstable, then the three-dimensional solution also approaches the limit cycle (figure 7.2(b)). $\square$

REMARK 6. *We observe that the solutions of the plane system, and in particular the limit cycle, are discontinuous with respect to ϕ. In particular, ϕ is discontinuous at $t = \hat{t}$, with $[\phi(\hat{t})] \neq 0$. The regularization of the solutions is done by connecting the discontinuity values of ϕ by a function $\bar{\phi}(\frac{t}{\mathcal{A}_4})$ that evolves according to the fast dynamics presented in the next section. For sufficiently small $\mathcal{A}_4$, the solutions of the three-dimensional system remain in $\mathcal{M}$ for most of the time, emerging to the third dimension in order to connect the separate branches $\mathcal{M}_1$ and $\mathcal{M}_2$, in the fast time scale. This is developed in section 9.*

8. Competitive systems and three-dimensional limit cycle. It is well known that for three dimensional systems, the compactness of a steady state free ω−limit set of an orbit is not sufficient to prove the existence of a periodic orbit. That is, the Poincaré-Bendixon theorem in its original form does not apply. However, a three-dimensional generalization is available for *competitive* (and *cooperative*) systems ([28], [29], [30], [34]). This concept is framed in terms of monotonicity properties of the vector field of the system with respect to a convex subspace of $\mathbb{R}^3$. The theorem is due to Hirsch and it is stated as follows:

THEOREM 8.1. *A compact limit set of a competitive or cooperative system in $\mathbf{R}^3$ that contains no equilibrium points is a periodic orbit.*

A dynamical system is called *competitive* in the positive cone $\mathbb{R}^{+^n}$ if $\frac{\partial f_i}{\partial x_j}(\mathbf{x}) \leq 0$, $i \neq j$, $\mathbf{x} \in \mathcal{I}$. This property holds in a general cone $\mathcal{K}$ (intersection of half-spaces), by requiring the following two properties:

DEFINITION 8.2. *A $n \times n$ Jacobian matrix $(\nabla \mathbf{f})$ is sign-stable in $\mathcal{I}$ if for each $i \neq j$, either $\frac{\partial f_i}{\partial x_j} \geq 0$ or $\frac{\partial f_i}{\partial x_j} \leq 0$, for all $\mathbf{x} \in \mathcal{I}$. It is sign-symmetric if $\frac{\partial f_i}{\partial x_j}(\mathbf{x})\frac{\partial f_j}{\partial x_i}(\mathbf{y}) \geq 0$ for all $i \neq j$ and for all $\mathbf{x}, \mathbf{y} \in \mathcal{I}$.*

PROPOSITION 8.3. *The three dimensional governing system (5.6)-(5.9) is competitive with respect to the cone $\mathcal{K} = \{(\phi, x, z) : \phi < 0, \ x > 0, \ z < 0\}$.*

The proof involves identifying $\mathcal{K}$ and verifying definition (8.2), which follows from these two lemmas.

LEMMA 8.4. *The inequalities $\phi(1-\phi)\frac{\partial \lambda}{\partial \phi} = \lambda \frac{fp}{\sqrt{1+p^2 f^2}} \geq \lambda$ and $\frac{\partial \lambda}{\partial x} < 0$ hold on trajectories $\boldsymbol{\varphi}_t$ corresponding to initial data in $\mathcal{I}$.*

Proof. For λ, p and f as in (5.9) and (5.14), simple calculations show that

$$\frac{2}{\gamma}(1-\phi)^2 \frac{\partial \lambda}{\partial \phi} = \frac{f}{\sqrt{1+p^2 f^2}} = \frac{f\lambda}{\sqrt{1+p^2 f^2}} = \frac{2}{\gamma}\frac{(1-\phi)}{\phi}\frac{fp\lambda}{\sqrt{1+p^2 f^2}},$$

$$\frac{\partial \lambda}{\partial x} = \frac{pf'}{\sqrt{1+p^2 f^2}}\lambda = -\frac{p}{(1+x)^2}\frac{\lambda}{\sqrt{1+p^2 f^2}} > -\frac{p}{(1+x)^2}\lambda, \tag{8.1}$$

from which the stated inequalities follow. $\square$

LEMMA 8.5. *The Jacobian matrix $\mathcal{J}$ of the three-dimensional system is sign-stable and sign-symmetric.*

Proof. Let us calculate the Jacobian matrix $J := \{a_{ij}\}$ at an arbitrary state (ϕ, x, z):

$$a_{12} = -(1-\phi)\phi^2 R'(\lambda)\frac{\partial \lambda}{\partial x}, \quad a_{21} = (1-\phi)(1+x)^2\frac{z}{2}\frac{\partial \lambda}{\partial \phi} - (1+x)^2(\frac{\lambda}{2}z - x), \tag{8.2}$$

$$a_{31} = -\beta e^{-\beta\phi} - \frac{\mathcal{A}_2}{\mathcal{A}_1}\big((1-\phi)z\frac{\partial \lambda}{\partial \phi} - (\lambda z - x)\big), \quad a_{13} = 0, \tag{8.3}$$

$$a_{23} = (1-\phi)(1+x)^2\frac{\lambda}{2}, \quad a_{32} = -\frac{\mathcal{A}_2}{\mathcal{A}_1}(1-\phi)(z\frac{\partial \lambda}{\partial x} - 1). \tag{8.4}$$

Note that the off-diagonal elements of the matrix J have the signs:

$$a_{12} > 0, \ a_{13} = 0, \ a_{23} > 0, \ a_{32} > 0, \ a_{21} > 0, \ a_{31} < 0.$$

from which, sign-symmetry and sign-stability immediately follow. For this, let us write

$$a_{21} = (1+x)^2\big((1-\phi)\frac{\partial \lambda}{\partial \phi}\frac{z}{2} - \frac{\lambda}{2}z + x\big) > \frac{x}{(1+x)^2} > 0. \tag{8.5}$$

Note that $a_{23} > 0$ and $a_{31} < -\beta e^{-\beta\phi} - \frac{\mathcal{A}_2}{\mathcal{A}_1}x < 0$, where we have used the first inequality in lemma 8.4. Finally, to check the sign of a_{12}, we differentiate $R(\lambda)$ in (5.13) to find $R'(\lambda) = (\sqrt{\lambda} - \frac{1}{\sqrt{\lambda}})(\lambda^{-\frac{1}{2}} + \lambda^{-\frac{3}{2}})$, from which the sign of a_{12} follows, taking into account the second inequality in lemma 8.4. The identification of the corresponding cone $\mathcal{K}$ is done in the Supplementary Material section. $\square$

One of the practical difficulties in the application of the Poincarè-Bendixon theorem to three-dimensional systems as compared to the two-dimensional counterpart is the verification that the ω-limit set does not contain equilibrium points. The case that the system has a single unstable equilibrium point is the simplest one to treat. Existence of a three dimensional limit cycle, together with additional properties of competitive systems relevant to the current analysis are summarized next.

THEOREM 8.6. *Let $\mathcal{P}, \mathcal{M}$ and $\mathcal{I}$ be as in definition (5.1), (7.8) and (5.19), respectively. Then*

1. *The flow on the ω-limit set of orbits of the three-dimensional system in $\mathcal{I}$ is topologically equivalent to the flow on the ω-limit set of orbits of the two-dimensional system in $\mathcal{M}$.*
2. *Let $\mathbf{p} = (\Phi, X, Z)$ be the unique equilibrium point of the system. If $\mathbf{p} \neq \mathbf{q} \in \mathcal{I}$, then $\mathbf{p} \notin \omega(\mathbf{q})$.*
3. *The three-dimensional system has a limit cycle.*

Proof. The first item follows from the fact that the two-dimensional system is Lipschitz, the competitiveness of the three dimensional system, and from the compactness of the ω-limit set of both systems. The second statement follows from competitiveness and the fact that the equilibrium point is unique and hyperbolic. In fact, it is a consequence of the theorem that states that *a compact limit set of a competitive or cooperative*

system cannot contain two points related by $<<$ ([34], Theorem 3.2). Finally, property (3) is a consequence of (2), the compactness of the ω-limit set and Theorem 8.1. $\square$

REMARK 7. *In the case that the unique equilibrium point $\mathbf{p}$ is hyperbolic, to prove that $\mathbf{p} \notin \omega(\mathbf{q})$, $\mathbf{q} \in \mathcal{D}$, it is necessary to assume that the system is competitive. This is the case encountered in some applications such as in virus dynamics [25].*

9. Multiscale Analysis. The analysis carried out in the previous sections is mostly based on the time scale separation between the mechanical and chemical evolution components of the system. In turn, this is based on the relative sizes of the dimensionless parameters $\mathcal{A}_i$. The goal of this section is to find estimates for the solutions of the three dimensional system with respect to the fast time scale. Let us consider the time scales $\bar{t}$ and τ as in (5.20), representing the *fast* and *slow* times, respectively. We consider the system of equations (5.21)-(5.23), together with (5.9)-(5.11). We propose the following solution ansatz

$$\phi(\bar{t}, \tau, \epsilon) = \Phi(\tau, \epsilon) + \tilde{\phi}(\bar{t}, \epsilon) = \Big(\sum_{j=0}^{N} \Phi_j(\tau) + \mathcal{E}_0^1 \Big) + \Big(\sum_{j=0}^{N} \tilde{\phi}_j(\bar{t}) + \mathcal{E}_I^1 \Big), \tag{9.1}$$

$$x(\bar{t}, \tau, \epsilon) = X(\tau, \epsilon) + \tilde{x}(\bar{t}, \epsilon) = \Big(\sum_{j=0}^{N} X_j(\tau) + \mathcal{E}_0^2 \Big) + \Big(\sum_{j=0}^{N} \tilde{x}_j(\bar{t}) + \mathcal{E}_I^2 \Big) \tag{9.2}$$

$$z(\bar{t}, \tau, \epsilon) = Z(\tau, \epsilon) + \tilde{z}(\bar{t}, \epsilon) + \Big(\sum_{j=0}^{N} Z_j(\tau) + \mathcal{E}_0^3 \Big) + \Big(\sum_{j=0}^{N} \bar{z}_j(\bar{t}) + \mathcal{E}_I^3 \Big), \tag{9.3}$$

with $\epsilon = \mathcal{A}_4$, $\bar{t} = \frac{\tau}{\epsilon}$, and $\mathcal{E}_0^j, \mathcal{E}_I^j$, $j = 1, 2, 3$, denote error terms. We now consider $\frac{\mathcal{A}_4}{\mathcal{A}_1}$ fixed and $0 < \epsilon << 1$. Equations for the terms in (9.1)-(9.3) are obtained as follows:
1. Holding τ fixed, and letting $\epsilon \to 0$ yields equations for Φ, X, Z. These are studied in section (7).
2. Holding $\bar{t}$ fixed, and letting $\epsilon \to 0$ yields equations for the initial layer term $\tilde{\phi}, \tilde{x}$ and $\tilde{z}$. Moreover, we seek solutions with the following asymptotic property $\{\tilde{\phi}(t, \epsilon), \tilde{x}(t, \epsilon), \tilde{z}(t, \epsilon)\} = O(\exp(-ct))$ as $t \to \infty$, where $c > 0$ is a material dependent parameter. Note that since X and Z satisfy initial conditions at $\tau = 0$, then $\tilde{x} = 0 = \tilde{z}$, and it is necessary to calculate only the initial layer for $\tilde{\phi}$.

9.1. Solutions in the fast time scale $\bar{t}$. To obtain equations for the initial layer terms, we substitute expressions (9.1)-(9.3) into the governing equations, fix $\bar{t} > 0$ and take the limit $\epsilon \to 0$. In particular, this yields the limit $\tau = 0$. Moreover, taking into account that $\mathcal{R}_1(\Phi, \Lambda) = -(1 - \Phi)\Phi^2 \big(R(\Phi) - H(\Lambda) \big) = 0$, and linearizing about (Φ, Λ) gives the following equation for $\tilde{\phi}(\bar{t}, \tau, \epsilon)$:

$$\frac{d\tilde{\phi}}{d\bar{t}} = -M(\Phi, \Lambda)\tilde{\phi}(\bar{t}, \epsilon) + o(\tilde{\phi}), \quad M(\Phi, \Lambda) := \frac{\partial \mathcal{R}_1}{\partial \phi}(\Phi, \Lambda) + \frac{\partial \mathcal{R}_1}{\partial \lambda}(\Phi, \Lambda)\frac{\partial \lambda}{\partial \phi}. \tag{9.4}$$

We point out that (Φ, Λ, Z) solve the two-dimensional system. To calculate the right hand side of (9.4), we take derivatives in equation (7.5), $\frac{\partial \lambda}{\partial \phi}(\Phi, X) = p'(\Phi)f(X) + q'(\Phi)$, $R'(\Lambda) = \gamma_0(1 - \frac{1}{\Lambda^2})$. So,

$$\begin{aligned} M(\Phi, \Lambda) &= -(1 - \Phi)\Phi^2 \big(H'(\Phi) - R'(\Lambda)(p'f(X) + q'(\Phi)) \big) \\ &= -\frac{1}{2}(1 - \Phi)\Phi^2 \big(H'(\Phi)(1 + \frac{1}{\Lambda^2}) - \frac{\gamma\gamma_0}{2(1 - \Phi^2)} f(X)(1 - \frac{1}{\Lambda^2}) \big). \end{aligned} \tag{9.5}$$

We point out that according to the earlier observation that (Φ, Λ) are evaluated at $\tau = 0$, it follows that the rate of decay of the fast component of the solution depends on the projection of the initial data on the slow manifold.

LEMMA 9.1. *Consider initial data $(\phi^0, \lambda^0, z^0) \in \mathcal{I}$ and let $M^0 := M(\phi^0, \lambda^+(\phi^0), z^0)$. If $M_0 > 0$, then the solution of the linear equation (9.4) satisfies $\tilde{\phi}(\bar{t}) = O(e^{-M^0\bar{t}})$, for $\bar{t} > 0$ large. Otherwise, $\tilde{\phi}(\bar{t}) = O(e^{|M_0|\bar{t}})$, for $\bar{t} > 0$ large.*

This lemma motivates the definition of *slow* and *fast* manifolds of the (three-dimensional) system. Let

$$\mathcal{S} = \{(\phi, \lambda, z) : \lambda = \lambda^+(\phi), M > 0\}, \quad \mathcal{F} = \mathcal{I}/\mathcal{S}, \tag{9.6}$$

with λ^+ as in (7.6). Note that the decomposition $\mathcal{S} \bigoplus \mathcal{F}$ corresponds to that in (9.1)-(9.3).
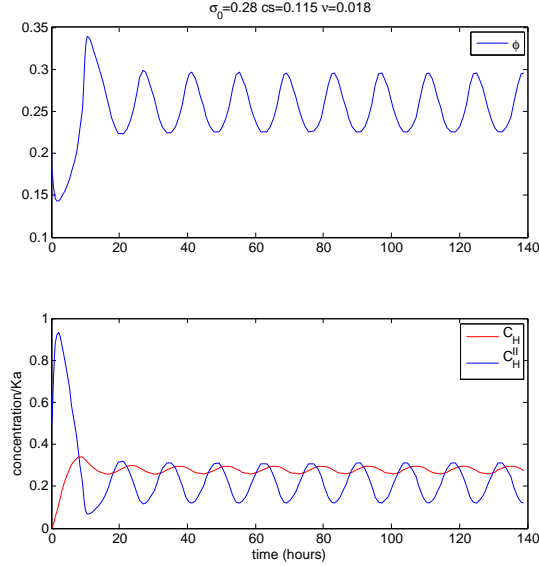
FIG. 9.1. *The top plot represents the swelling dynamics of the membrane in terms of the polymer volume fraction. The graphs of the bottom plot refer to the evolution of H^+ in the membrane (red) and in cell II (blue), respectively. The oscillatory behavior is compatible with the GnRH pulse release.*

REMARK 8. *Note that a sufficient condition for $M^0 > 0$ is that $H'(\phi^0) \leq 0$, that is $\phi^0 \in \mathcal{N}^-$. So, the first inequality may still hold in the case that $H'(\phi^0) > 0$, that is, for $\phi_0 > \phi_{min}$ or $\phi_0 < \phi_{max}$ in figure 5.1. This property is referred to as the reduced system having a canàrd structure [7, 8]. The case $M = 0$ cannot be characterized in terms of linear stability.*

THEOREM 9.2. *Let $(\phi^0, x^0, z^0) \in \mathcal{I}$ and suppose that the parameters of the system belong to the class $\mathcal{P}$. Then there exists $\epsilon_0 > 0$ such that for $\epsilon \in (0, \epsilon_0)$ the governing system has a unique C^1-solution $(\phi(t; \epsilon), x(t; \epsilon), z(t; \epsilon)) \in \mathcal{I}$, for all $t > 0$. Moreover $(\phi(\cdot), \lambda(\cdot), z(\cdot)) \in \mathcal{S} \bigoplus \mathcal{F}$ and it admits the asymptotic expansions (9.1), (9.2) and (9.3), with the property that $\mathcal{E}_0^k = O(\epsilon^N)$, $\mathcal{E}_I^k = O(e^{-M_0 \bar{t}})$, $k = 1, 2, 3$, for sufficiently large $\bar{t}$.* The proof follows from linearization of the three-dimensional system with respect to solutions of the two dimensional one, subsequently transforming it into a system of integral equations, and applying Schauder's fixed point theorem to it.

REMARK 9. *We consider the model obtained by further reducing the time scale, that is, setting the limiting problem in the slow scale as $0 = \mathcal{R}_1(\phi, \lambda)$, $\frac{d\bar{x}}{d\tau} = \mathcal{R}_2(\phi, \bar{x}, \lambda)$, $0 = \mathcal{R}_3(\phi, \bar{x}, \bar{z}, \lambda)$, together with equations (5.9). This is consistent with taking $\frac{\mathcal{A}_4}{\mathcal{A}_1} = O(\epsilon^{-3})$. This model yields that proposed by Siegel and Li [5], that sets a rely equation for the product of the reaction, in this case, the hydrogen ion concentration in the membrane.*

10. Concluding Remarks. We have analyzed a *lumped* model for a chemomechanical oscillator suitable for rhythmic drug delivery. The model consists of a system of ordinary differential equations for the chemo-mechanical fields. For this system, we showed existence of periodic solutions, which correspond to experimentally and numerically observed oscillations. The tools of the analysis involve multiscale and dynamical systems methods, including the theory of competitive dynamical systems [28].

The membrane model, which ignores gradients of solute concentrations and swelling within the membrane, can be replaced by a distributed, PDE based system which, in addition to more accurately portraying the physical situation, can include self consistent, natural boundary conditions at the interfaces between the membrane and the two chambers. The results presented here will not be altered qualitatively, though there will be quantitative differences.

Overall, the model presented here dealt with the fundamental mechanisms underlying oscillatory behaviour of a table-top experimental device. It must be regarded as a first step, since complications associated with the buildup of gluconate ion in the system, which buffers and affects the dynamics of pH oscillations, have not been included. Also the effects of endogenous phosphate and bicarbonate buffering species would need to be included in a more comprehensive model, which would be of higher dimensionality, even in the lumped framework. These buffering effects are currently the main hurdle to develop an in-vivo device.

REFERENCES

[1] A. ADRONOV, A. VITT, AND S. KHAIKHIN, *Theory of Oscillators*, Dover, New York, 1966.

[2] A.P.DHANARAJAN, G.P.MISRA, AND R.A.SIEGEL, *Autonomous chemomechanical oscillations in a hydrogel-enzyme system driven by glucose*, The Journal of Physical Chemistry A, 106 (2002), pp. 8835–8838.

[3] A.S.BHALLA AND R.A.SIEGEL, *Mechanistic studies of an autonomously pulsing hydrogel-enzyme system for rhythmic hormone delivery journal of controlled release*, J. Control. Rel., 196 (2014), pp. 261–271.

[4] B.A.FIRESTONE AND R.A.SIEGEL, *Dynamic ph-dependent swelling properties of a hydrophobic polyelectrolyte gel*, Polym. Commun., 29 (1988), pp. 204–208.

[5] B.LI AND R.A.SIEGEL, *Global analysis of a model pulsing drug delivery oscillator based on chemomechanical feedback with hysteresis*, Chaos, 10 (2000), pp. 682–690.

[6] B.M.CHABAUD AND M.C.CALDERER, *Effects of permeability and viscosity in polymer gel models*, Math.Meth.Appl. Sci, Accepted for Publication (2014).

[7] K. BOLD, C.EDWARDS, J. GUCKENHEIMER, S. GUHARAY, K.HOFFMAN, J. HUBBARD, R.OLIVA, AND W. WECKESSER, *The forced van der pol equation: Canards in the reduced system*, SIAM J. Dyn. Systems, 2 (2003), pp. 570–608.

[8] B.PENG, V.GASPAR, AND K.SHOWALTER, *False bifurcations in chemical systems*, Phil. Trans. Royal Soc. A, 337 (1991), pp. 275–289.

[9] A. P. DHANARAJAN, *Mechanistic studies and development of a hydrogel-enzyme drug delivery oscillator*, in Doctoral dissertation, University of Minnesota, 2004, pp. 1–178.

[10] A. ENGLISH, T. TANAKA, AND E. EDELMAN, *Polyelectrolyte hydrogel instabilities in ionic solutions*, Journal of Chemical Physics, 17 (1996), pp. 10606–10613.

[11] I. EPSTEIN AND J. POJMAN, *An Introduction to Nonlinear Chemical Dynamics*, Oxford, New York, 1998.

[12] B. ERMAN AND P. FLORY, *Critical phenomena and transitions in swollen polymer networks in and linear macromolecules*, Macromolecules, 19 (1986), pp. 2342–2353.

[13] P. FLORY, *Principles of Polymer Chemistry*, Cornell, Ithaca, N.Y., 1953.

[14] A. GOLDBETER, *Biochemical Oscillations and Cellular Rhythms*, Cambridge University Press, Cambridge, UK, 1996.

[15] G.P.MISRA AND R.A.SIEGEL, *Hypophysial responses to continuous and intermittent delivery of hypothalamic gonadotropin-releasing hormone*, Journal of Controlled Release, 81 (2002), pp. 1–6.

[16] P. GRAY AND S. SCOTT, *Chemical Oscillations and Instabilities*, Clarendon, Oxford, U.K., 1990.

[17] P. GRIMSHAW, J. NUSSBAUM, A. GRODZINSKY, AND M. YARMUSH, *Kinetics of electrically and chemically induced swelling in polyelectrolyte gels*, The Journal of Chemical Physics, 93 (1990), p. 4462.

[18] S. HIROTSU, *Static and time-dependent properties of polymer gels around the volume phase transition*, Phase Transitions, 47 (1994), pp. 183–240.

[19] J.E.MARSDEN AND M.MCCRAKEN, *The Hopf Bifurcation and its Applications*, Springer-Verlag, 1976.

[20] J.K.HALE, *Ordinary Differential Equations*, John Willey, 1980.

[21] J.P.BAKER AND R.A.SIEGEL, *Hysteresis in the glucose permeability versus ph characteristic for a responsive hydrogel membrane*, Macromol. Rapid. Commun, 17 (1996), pp. 409–415.

[22] J.RICKA AND T.TANAKA, *Swelling of ionic gels: Quantitative performance of the donnan theory*, Macromolecules, 17 (1984), pp. 2916–2921.

[23] A. KATCHALSKY, *Polyelectrolyte gels*, Progress in Biophysical Chemistry, 4 (1954), pp. 1–59.

[24] C. LAMAZE AND E. PETERLIN, *Diffusion and hydraulic permeabilities of water in water-swollen polymer membranes*, J.Poly.Sci. Pt A-2, 9 (1971), p. 1117.

[25] P. LEENHEER AND H.L.SMITH, *Virus dynamics: a global analysis*, SIAM Journal Math. Analysis, 63 (2003), p. 1313.

[26] R. MACOMBE, S. CAI, W. HONG, X. ZHAO, Y. LAPUSTA, AND Z. SUO, *A theory of constrained swelling of a ph-sensitive hydrogel*, Soft Matter, 6 (2010), pp. 784–793.

[27] H. F. MARK AND J. I. KROSCHWITZ, *Encyclopedia of polymer science and engineering.*, Nečas, 1980.

[28] M.W.HIRSH, *Systems of differential equations which are competitive or cooperative. i: Limit sets*, SIAM Journal Math. Analysis, 13 (1982), pp. 167–179.

[29] ———, *Systems of differential equations which are competitive or cooperative. ii: Convergence almost everywhere*, SIAM Journal Math. Analysis, 16 (1985), pp. 423–439.

[30] ———, *Systems of differential equations which are competitive or cooperative. iv: Structural stability in three-dimensional systems*, SIAM Journal Math. Analysis, 21 (1990), pp. 1225–1234.

[31] N. PEPPAS, *Hydrogels in Medicine and Pharmacy*, CRC Pressl, Boca Raton, Fl., 1986.

[32] J. RICKA AND T. TANAKA, *Swelling of ionic gels: Quantitative performance of the donnan theory*, Macromolecules, 17 (1984), pp. 2916–2921.

[33] J. SIEPMANN, R. SIEGEL, AND M. RATHBONE, eds., *Fundamentals and Applications of Controlled Release Drug Delivery*, Springer, New York, 2012.

[34] H. SMITH, *Monotone Dynamical Systems*, vol. 41, AMS, 1995.

[35] H. YASUDA, C. LAMAZE, AND E. PETERLIN, *Salt rejection by polymer membranes in reverse osmosis. ii. ionic polymers*, J.Poly.Sci. Pt A-2, 9 (1971), p. 1579.